A STUDY OF ADSORPTION OF SINGLE ATOMS ON CARBON NANOTUBES

A THESIS

SUBMITTED TO THE DEPARTMENT OF PHYSICS

AND THE INSTITUTE OF ENGINEERING AND SCIENCE

OF BILKENT UNIVERSITY

IN PARTIAL FULFILLMENT OF THE REQUIREMENTS

FOR THE DEGREE OF

MASTER OF SCIENCE

By

Engin Durgun

September, 2003

I certify that I have read this thesis and that in my opinion it is fully adequate, in scope and in quality, as a thesis for the degree of Master of Science.

Prof. Dr. Salim Çıracı (Advisor)

I certify that I have read this thesis and that in my opinion it is fully adequate, in scope and in quality, as a thesis for the degree of Master of Science.

Prof. Dr. Atilla Erçelebi

I certify that I have read this thesis and that in my opinion it is fully adequate, in scope and in quality, as a thesis for the degree of Master of Science.

Prof. Dr. Şakir Erkoç

Approved for the Institute of Engineering and Science:

Prof. Dr. Mehmet B. Baray
Director of the Institute Engineering and Science

ABSTRACT

A STUDY OF ADSORPTION OF SINGLE ATOMS ON CARBON NANOTUBES

Engin Durgun
M.S. in Physics
Supervisor: Prof. Dr. Salim Çıracı
September, 2003

The adsorption of individual atoms on the semiconducting and metallic single-wall carbon nanotubes (SWNT) have been investigated by using first-principles pseudopotential plane wave method within Density Functional Theory. The stable adsorption geometry and binding energy have been determined for a large number of foreign atoms ranging from alkali and simple metals to the transition metals and group IV elements. We have found that the character of the bonding and associated physical properties strongly depend on the type of adsorbed atoms, in particular on their valence electron structure. Our results indicate that the properties of SWNTs can be modified by the adsorbed foreign atoms. While the atoms of good conducting metals, such as Zn, Cu, Ag and Au, form very weak bonds, transition metal atoms, such as Ti, Sc, Nb and Ta, and group IV elements C and Si are adsorbed with relatively high binding energy. Owing to the curvature effect, these binding energies are larger than the binding energies of the same atoms on the graphite surface. We have showed that the adatom carbon can form strong and directional bonds between two SWNTs so that the tubes are connected. These connects can be used to produce nanotube networks or grids. Most of the adsorbed transition metal atoms excluding Ni, Pd and Pt have a magnetic ground state with a significant magnetic moment. Our results suggest that carbon nanotubes can be functionalized in different ways by their coverage with different atoms, showing interesting applications such as one-dimensional nanomagnets or nanoconductors and conducting connects etc.

Keywords: ab initio, first principles, carbon nanotube, density functional theory, adsorption, binding, metal, coating.

ÖZET

KARBON NANOTÜPLERDE TEK ATOM SOĞURULMASININ İNCELENMESİ

Engin Durgun
Fizik , Yüksek Lisans
Tez Yöneticisi: Prof. Dr. Salim Çıracı
Eylül, 2003

Bu çalışmada çok sayıda yabancı atom için temel prensiplerden başlayarak ve durum yoğunluğu teorisi kullanılarak, tek atomun yarı iletken ve metalik tek duvarlı karbon nanotüp (TDNT) üzerinde soğurulması incelenmiştir. Alkali ve basit metallerden, geçiş metalleri ve Grup IV elementlerine kadar bir çok atomu içeren bir alanda kararlı soğurulma geometrileri ve bağlanma enerjileri analiz edilmiştir. Bağlanma karakterinin ve buna bağlı fiziksel özelliklerin soğurulan atomun türüne ve elektron yapısına bağlı olduğu anlaşılmıştır. TDNT'nin özelliklerinin soğurulan atomla birlikte fraklı özellikler gösterdiği gözlenmiştir. İyi iletkenlik özelliği gösteren Zn, Cu, Ag ve Au gibi metaller zayıf bağ yaparken; Ti, Sc, Nb ve Ta gibi geçiş metalleri ile C ve Si gibi Grup IV elementlerinin oldukça kuvvetli bağlar oluşturduğu anlaşılmıştır. Soğurulan C atomunun iki TDNT arasında kuvvetli ve yönlü bağ oluşturarak bu iki tüpün birleşmesini sağladığı görülmüştür. Ni, Pd ve Pt dışındaki geçiş metallerinin manyetik taban düzeyine sahip olduğu ve bu düzeylerin manyetik momentlerinin oldukça yüksek değerde olduğu tesbit edilmiştir. Elde ettiğimiz sonuçlar nanotüplerin değişik atomlarla kaplanarak ilginç özellikler kazanabileceğini ve bu özellikler sayesinde bir boyutlu nano-mıknatıslar, nano-iletkenler ve quantum teller gibi uygulamalarda kullanılabileceğini öngörmektedir.

Anahtar sözcükler: ab initio, temel prensipler, karbon nanotüp, durum yoğunluğu teorisi, soğurulma, bağlanma, metaller, kaplama.

Acknowledgement

I would like to express my deepest gratitude and respect to my supervisor Prof. Dr. Salim Çıracı for his patience and guidance during my study and also for giving me a chance to be one of his assistant.

I am thankful to Dr. Oğuz Gülseren for his valuable discussions and advices.

I appreciate Prof. Dr. Ekmel Özbay for his motivation and interest beginning from Freshman year. His advices and motivation kept me standing in this area.

I also remember Dr. Ahmet Oral for the days I spent in Advanced Research Laboratory.

My sincere thanks due to Dr. Ceyhun Bulutay for his moral support and guidance.

I would like to thank to Sefa Dağ for being my partner, office-mate and home-mate.

I would also thank to my ex-home-mate Ertuğrul Çubukçu being one of my closest friend during last six years in Bilkent.

I would never forget the help and motivation of Cem Sevik, Deniz Çakir, Sefaattin Tongay, Yavuz Öztürk and Ayhan Yurtsever during my hard times.

I would like to thank to all my friends in Physics Department for their friendship.

I bless to my mother and father for their endless love and support.

I would like to thank to my only brother for being my closest friend and guide beginning from my childhood and to his dear wife for being my missing sister.

And finally I would like thank my intended wife, Nalan for her motivation, moral support and endless trust in me all the times...

Contents

List of Figures

List of Tables

Chapter 1

Introduction

Carbon materials are found in various forms such as graphite, diamond, carbon fibers, fullerenes, and carbon nanotubes. Requirements for novel materials of particular properties such as durability, elasticity etc., was the reason of early interests cast on carbon fibers, both in the 19^{th} century and after the World War II. It was Thomas A. Edison who first invented and prepared a carbon fiber, in order to provide a filament for an early model of an electric light bulb [1]. In spite of the fact that the pioneering work came at a respectively earlier time, it was not until fifties that a following study came. The needs in space and aircraft industry urged researchers to come up with a second application in this field. In parallel to ongoing scientific studies, other research studies focused on control of the process for the synthesis of vapor grown carbon fiber [2, 3], which leaded to current commercialization of vapor grown carbon fibers in nineties for various applications. The growth of very small diameter filaments was occasionally observed and reported, as researches on vapor grown fibers on the micrometer scale proceeded. Reports of such thin filaments inspired Kubo to ask whether there was a minimum dimension for such filamnets. Direct motivation for studying carbon filaments of very small diameters more systematically came from the discovery of fullerenes by Kroto and Smalley [4]. In December 1990, inspired by the discussions on studies of Huffmann and Dresselhaus [5], Smalley spoke of the existence of carbonic tubes of dimensions comparable to C_{60} (Bucky Ball). However, the

real breakthrough on carbon nanotube research come with Iijima's report of experimental observation of carbon nanotubes(CNTs) using transmission electron microscopy [6]. It was this work which connected the experimental observations with the theoretical framework of carbon nanotubes in relation to fullerenes and as a theoretical model of 1D systems. After this revolutionary observation of Iijima the study of CNTs has progressed rapidly.

CNTs are unique materials which offer a variety of structural parameters to engineer their physical and chemical properties [7, 8]. They can be synthesized as single wall (SWNT) or multiple wall (MWNT) nanotubes; they can form ropes or even crystals. SWNTs are basically rolled graphite sheets, which are characterized by two integers (n, m) defining the chiral vector $\mathbf{C} = n\mathbf{a}_1 + m\mathbf{a}_2$, in terms of the two-dimensional (2D) hexagonal Bravais lattice vectors of graphene, $\mathbf{a}_1$ and $\mathbf{a}_2$. Nanotubes have radius and structure dependent physical properties [9, 10]. They can be either metallic and semiconducting depending on the chirality and radius, in other words depending on n and m. In the last decade, extensive research have been carried out on SWNTs aiming at the modification of electronic structure for desired device operations.

The mechanical properties of carbon nanotubes are striking. They are flexible and can sustain large elastic deformations radially, at the same time are very strong with high yield strength [11, 12], that is, it is easy to apply elliptical deformations but is very difficult to elongate the system. Their strength far exceeds that of any other fiber. Even more striking is the response of electronic structure to the radial deformation leading dramatic changes. As it has been predicted theoretically and confirmed experimentally, a semiconducting zigzag tube becomes metallic with finite state density at the Fermi level as a result of radial deformation transforming the circular cross section into an ellipse. At the same time chemical activity of the surface of the tube undergoes a change; the interaction of adatoms with the SWNT occurs differently at high- and low-curvature sites. Metal-semiconductor transition induced by an elastic deformation has important implications.

Physical properties of a SWNT can also be modified by the adsorption of

foreign atoms or molecules. This process is usually named as functionalization, and carries a great potential in constructing new nanostructures and to engineer them according to a desired application. For example, depending on the pattern of hydrogen atom coverage, while a metallic armchair SWNT is transformed to a wide-band gap semiconductor, a semiconducting zigzag tube becomes a metal with very high state density [13, 14]. A free SWNT, which is normally non-magnetic, becomes magnetic with unpaired spins upon the adsorption of oxygen molecule or specific transition metal atoms [15]. A recent study demonstrates that a semiconducting zigzag tube becomes both magnetic and high-conductance wire as a result of Ti coating [16].

One of the grand challenges of research on carbon nanotubes has been the realization of nanometer optoelectronic devices and nanomagnets. In an effort to discover a new feature which may be of technological interest, several theoretical and experimental studies actively explored SWNTs, MWNTs, ropes and their functionalized forms. Therefore, the study on nanotubes has seen a tremendous explosion.

A few interesting works may give the reader idea about the endless applications and help to understand the physical interest on CNTs:

The use of nanotubes in technologies related to microscopy is one of the application area. CNTs are mechanically strong, chemically inert, and have a large aspect ratio (quasi 1-Dimensional system). All these properties make CNTs at least in principle a well-defined tip which can be used for Scanning Probe Microscope (SPM) and Atomic Force Microscopy (AFM). Dai et al. [17] pioneered the use of nanotubes for scanning probe microscope (SPM) tips at Rice University. Aranson [18] has demonstrated that the use of nanotubes as a tip enhanced the resolution for electrostatic microscopy.

CNTs show great promise for nanoscale field-effect transistors (FET) [19]. Heinze et al. show that whenever there is a substantial Schottky barrier (SB) at the contact, CNT-FETs operate as unconventional Schottky barrier transistors, in which switching occurs primarily by modulation of the contact resistance rather than the channel conductance. SB-FETs have already been considered

as a possible future silicon technology because of their potential to operate at extremely small dimensions [20].

The use of CNTs as field-emitter tips is an another promising application. Saito at Mie University in Japan developed cathode-ray tubes equipped with nanotube field emitters [19]. This study has awoken the possibility of replacing the metallic emitter tips with CNT field emitters.

Recently, transport measurements performed in SWNT ropes show evidence of resonant tunneling through quantized energy levels [21] and quantum dot (QD) behavior have been observed [22]. In these experiments, energy quantization is due to the presence of the metallic contacts needed to conduct the measurements. Such findings stimulate the exploration of other possible devices based on carbon, aiming at the design of nanotube-based nanoelectronics. In principle, one can expect that a quantum dot can be obtained by combining two CNT metal-semiconductor junctions. This structure behaves as an ideal zero-dimensional (0D) device, presenting well-separated discrete levels and unexpected features which can be related to the CNT band structure.

A metallic wire formed from a single molecule is very unusual. In 1930, Rudolf Pierls showed that 1-D metallic wires are essentially unstable and will turn semiconducting [23]. Nanotubes are an exception to this general rule. Because of the tubular structure, the energy change of setting up a Pierls distortion is very unfavorable and there exists a metallic state in CNTs as a 1-D system. In metallic nanotubes, two of the subbands cross the Fermi level, and all of the current is predicted to be carried by only this pair. As each subband can in principle support a conductance of $G_0 = 2e^2/h$, which is known as the conductance quantum, one expects a conductance of $2G_0$ for metallic nanotubes. On the other hand resistance measurements yielded a resistance from 100 MΩ to several GΩ [24]. According to the fulfilled experiments the resistance of a SWNT at a length of 1 μm is predicted as 1-100 kΩ. Then the resistivity values for metallic CNTs are order of $10^{-5}\Omega$cm which is comparable with that of a typical metal. CNTs are thus predicted to be prototype 1-D quantum wires.

In order to fabricate tiny and fast device having low power dissipation, low

contact resistance between each component is needed. Previously produced metal-CNT contact with Pb and Au yielded a high resistance changing from $1M\Omega$ to $4M\Omega$ which was much larger than the typical metal-metal contact. (A typical metal-metal contact resistance will of the order of quantum resistance which is $13k\Omega$) A contact resistance as low as $13k\Omega$, which is sought for device fabrication, is finally reported for Ti contacted metallic SWNT [25].

The novel properties of CNTs can further be developed by coating the walls of nanotubes by proper metal [26]. The conductance of bare nanotube can be increased and electronic properties can be designed by this method. There exists reports on Au, Pd, Fe, Al, Pb, and Ti coated nanotubes. in these studies it is pointed out that metal-nanotube and metal-metal interactions play the important role for the coating problem. Depending on these interactions metal coatings altered in smoothness and in shape for each. Single atom studies may helpful for predicting and understanding these interactions [13]. Among all the metals coated, Ti coating yielded the most smooth one. The coating was continuous and uniform for various thicknesses. Such kind of nanowires may play a crucial role in future devices.

As a final remark, NASA and the Johnson Space Center (JSC) have made a commitment to pursue and drive breakthrough technologies to expand human exploration of space. They declared that the very future of space exploration depends on advanced technologies such as nanotechnology and biomimetics. Toward this goal, JSC is focusing on the development of nanotechnology based on single-wall carbon nanotubes. JSC is working toward bulk SWNT production methods to reduce cost and foster widespread applications studies. NASA's commitment to nanotechnology is testimony that nanoscopic materials, nanoelectronics and molecular devices will also be crucial for future space exploration.

1.1 Summary of Various Research Projects including Carbon Nanotubes

- Controlled Drug Delivery/release
- Conducting Composites
- Micro-electronics / semiconductors
- Artificial Muscles
- Supercapacitors
- Batteries and Fuel Cells
- Field emission flat panel displays
- Field Effect Transistors and Single Electron Transistors
- Nano-lithography
- Nano-electronics
- Doping
- Nano-balance
- Nano-tweezers
- Data-storage
- Magnetic Nanotubes and Nanomagnets
- Nano-gear
- Nanotube actuators
- Molecular Quantum Wires
- Hydrogen Storage
- Noble Radioactive Gas Storage

- Solar Storage
- Waste Recycling
- Electromagnetic Shielding
- Dialysis Filters
- Thermal Protection
- Nanotube Reinforced Composites
- Reinforcement of Polymers
- Avionics
- Spintronics
- Collision-Protection Materials
- Fly wheels
- Space projects
- Quantum Computation

1.2 Motivation

Research on carbon nanotubes is ever intensifying in diverse fields of science and engineering in spite of twelve years passed since its first discovery by Iijima [6]. There are several reasons why so much interest has focused on these materials. First of all, carbon nanotubes have been a natural curb for the several research programmes, which were tuned to C_{60} but all of a sudden came to an end without any great technological application so far. Secondly, researchers, who can touch and relocate atoms, have been challenged to discover the novel properties of these strange materials in order to transform them to new devices or other technological applications. As a result of rapid rise in the speed, as well as rapid reduction in the size of electronic devices, new paradigms have been needed to overcome

the barriers set by the traditional technologies to produce ever smaller and faster devices. Nanoelectronics based on carbon nanotubes have been considered as a new frontier aiming at the ultimate miniaturization of electronic circuits with ultra high density components and new functionalities. Several devices fabricated so far with different functionalities hold the promise of great expectations from carbon nanotubes.

1.3 Organization of the Thesis

The thesis is organized as follows: Chapter 2 summarizes the basic properties of CNTs, Chapter 3 focuses on the theoretical background and approximation methods. In Chapter 3, our studies are presented and emerging results are discussed. And finally in Chapter 4, a brief conclusion summaries the result of our studies and suggests possible future works.

Chapter 2

Carbon Nanotubes

Carbon nanotube (CNT) is a macro-molecule of carbon which is analogous to a single layer of graphite (graphene) rolled into a cylinder which has a diameter as small as 1 nanometer and a length up to many microns (see Fig. 2.1).

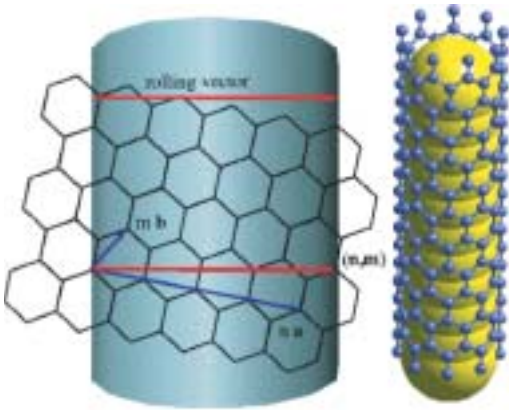

Figure 2.1: Carbon nanotube is a single layer of graphite rolled into a cylinder.

Each end of cylinder capped with half of a fullerene molecule. In the ideal case, a CNT consists of either one cylindrical graphene sheet (single-wall nanotube, SWNT) or of several enclosed cylinders with an interlayer spacing of 0.34 - 0.36 nm (multiwall nanotube, MWNT). Therefore, SWNTs can be viewed as the fundamental cylindrical structure which also form the building blocks of both

MWNTs and the nanoropes. Many theoretical studies have revealed the novel properties of SWNTs.

2.1 Graphene

Graphite is a 3-D layered hexagonal lattice of carbon atoms. A single layer of graphite is called 2-D graphite or graphene layer. Even in 3-D graphite, the interaction between two adjacent layers is small compared with intra-layer interactions. Thus, the electronic structure of 2-D graphite is first approximation of that for 3-D graphite.

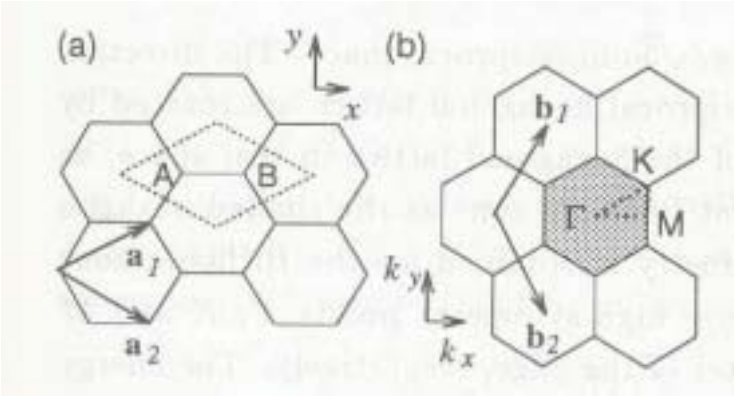

Figure 2.2: (a) The unit cell and (b) Brillouin zone of graphene are shown as the dotted rhombus and the shaded hexagon, respectively. $\mathbf{a_i}$ and $\mathbf{b_i}$ (i=1,2) are unit vectors and reciprocal lattice vectors respectively. Γ, K and M are high symmetry points.

In Fig. 2.2, the unit cell and the Brillouin zone of graphene is shown. If the shaded hexagon in Fig 2.2 is selected as the first Brillouin zone, the highest symmetry is obtained for the graphene. The high symmetry points Γ, K, M are defined as the center, the corner, and the center of the edge respectively.

In Fig. 2.3 the energy dispersion relation along the high symmetry axis is shown. The upper half of the energy dispersion curve describes the π^*-energy-anti-bonding band, and the lower half is the π-energy bonding band. The upper

and lower band are degenerate at the K points through which the Fermi energy passes. Only π-bands are considered since π energy bands are covalent and they mostly determine the solid state properties of graphene.

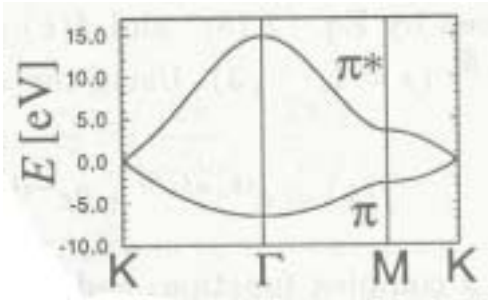

Figure 2.3: The energy dispersion along the high symetry directions of the triangle ΓML.

2.2 Structure of CNTs

The structure of CNTs have been explored by using the high resolution microscopy techniques. The cylindrical structures based on the hexagonal lattice of carbon atoms have been confirmed. There exist three types of nanotubes which are called armchair, zigzag and chiral depending on the rooling angle of graphene sheet(See Fig. 2.4). Different types are distinguished in terms of the unit cell of the tube. The chiral vector ($\mathbf{C_h}$) of the nanotube is defined by $\mathbf{C_h} = \mathrm{n}\mathbf{a_1} + \mathrm{m}\mathbf{a_2}$ which is specified as (n,m), here $\mathbf{a_1}$ and $\mathbf{a_2}$ are unit vectors of the graphene, and n and m are positive integers including zero (See Fig. 2.5). The $\mathbf{C_h}$ of the nanotube is determined on a graphene layer. When the graphene sheet is rolled up to build the nanotube, ends of the $\mathbf{C_h}$ meet each other, thus $\mathbf{C_h}$ also forms the circumference of the nanotube's circular cross-section. The different values of n and m lead to different nanotube structures. If $n = m$ and hence the chiral angle is 30^o the nanotube is called armchair. Zigzag nanotubes are formed when either n or m are zero and the chiral angle is 0^o. Nanotubes, having chiral angles between 0^o and 30^o, are known as chiral nanotubes. (Due to the symmetry of hexagons, the structures repeat themselves for angles greater than 30^o) The diameter and chiral

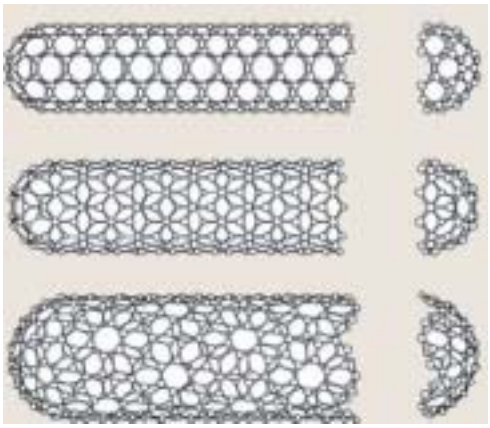

Figure 2.4: A (5,5) armchair nanotube (top), a (9,0) zigzag nanotube (middle) and a (10,5) chiral nanotube.

angle, in other words the indices n and m determine the properties of nanotubes. The diameter, d_t, is given by L/π, in which L is the circumferential length of the carbon nanotube:

$$d_t = \frac{C_h}{\pi} = a\sqrt{n^2 + m^2 + nm} \tag{2.1}$$

where $a(2.49A^o)$ is the lattice constant of honeycomb lattice.

2.3 Unit cells in Real and Reciprocal Space

The unit cell of a CNT in real space is given by the rectangle generated by chiral vector and the translational vector **T**. For graphite two translational vectors are needed; one vector in each dimension. CNTs are 1-D objects. Therefore only one translational vector, called **T** is sufficient. It is along the tube axis direction and is perpendicular to the circumference.

The unit cell of CNT has 2N carbon atoms where N is the number of hexagons. This means, there will be N pairs of bonding π and anti-bonding π^* electronic energy bands.

If the unit cell of a nanotube is x times larger than that of a hexagon, the

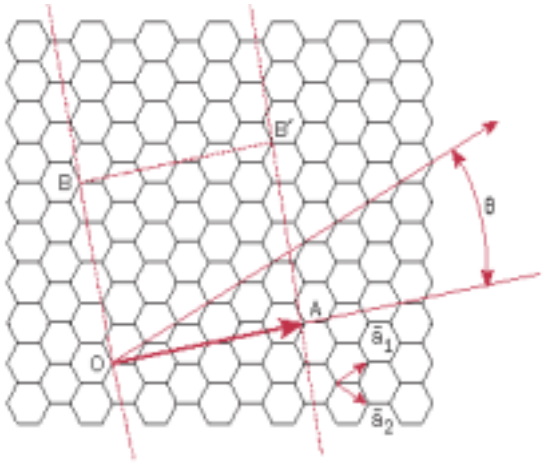

Figure 2.5: The chiral vector, chiral angle and unit vectors on the hexagonal lattice.

unit cell of the nanotube in reciprocal space is $1/x$ times smaller than that of a single hexagon.

2.4 Electronic Properties

In CNTs, the carbon atoms contain an sp^2 hybridization. There are 4 valence electrons for each carbon atom. The first three electrons belong to the σ orbital and are at energies -2.5 eV below the Fermi Level. Therefore, at low temperatures they are not expected contribute to electrical conduction. The fourth valence electron is located in the π orbital, which is slightly below the Fermi Level(E_F), thus this electron is responsible from transport.

CNTs are also predicted to be ideal 1-D quantum wires, since the diameter of the tube is smaller then the electronic de Broglie wavelength. Moreover, owing to almost perfect regularity of the atomic structure the mean free path of the electrons in the tube is much greater than the atom spacing in the lattice. Therefore, the electrons should contain very high mobility which is an attractive characteristic for nanoconductors.

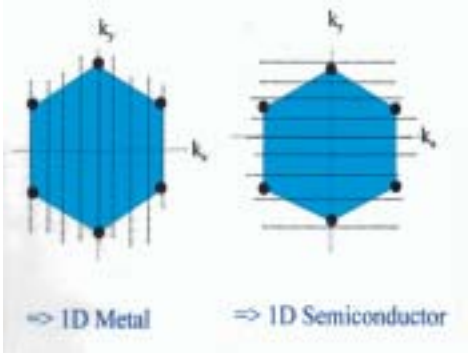

Figure 2.6: Zone folding in the graphene's first Brillouin zone for armchair and zigzag tubes.

The conduction of the CNT was analyzed first by using a 1-D tight binding method [27]. Those theoretical studies ,have been confirmed later by experiments, and showed that nanotubes could be either metallic or semiconducting. The band structure of CNTs can be understood by zone folding of the graphene bands in the hexagonal Brillouin zone(See Fig. 2.6). Simple relations stating that if: $n = m$ (armchair) or $n - m$ is divisible by three, CNTs become metallic, If $n - m$ is not divisible by three, CNTs show semiconducting behavior with a energy gap of ranging from 0.2 eV to 1 eV.

As the diameter of CNT increases, more wavevectors are allowed in the circumferential direction and the band gap in semiconducting nanotubes decreases. The band gap approaches zero at large diameters like a graphene sheet.

The unique electronic properties of CNTs are influenced by the quantum confinement of electrons normal to the axis. In the radial direction, electrons are confined in a monolayer thickness of the graphene sheet. Around the circumference of the nanotube, periodic boundary condition comes into play. As a result, electrons can only propagate along the nanotube axis, and so their wavevectors point in this direction. The resulting number of 1-D conduction and valence bands depend on the standing waves that are set up around the circumference of the nanotube.

Electron-electron interactions, mixing of bonding and anti-bonding orbitals during curvature of tube, and the Pierls [23] distortion, which are predicted to create a gap in metallic wires have not been observed experimentally in SWNTs.

2.5 Synthesis of Carbon Nanotubes

There are two main methods to synthesize SWNT‘s. The first one is laser vaporization. This is a method for the synthesis of bundles of SWNT‘s with a narrow diameter(See Fig. 2.7). In early works [28] high yields of 70-90% conver-

Figure 2.7: Pictures taken from Schönenberger‘s Group

sion of graphite to SWNT‘s were reported. A Co-Ni/graphite composite target and a temperature higher than 1000^oC is needed for this technique. The second method is arc-discharge, where SWNT‘s, and MWNT‘s, are grown [29, 30]. The carbon arc provides a simple and traditional tool for generating the high temperatures, higher than 3000^oC, needed for the vaporization of carbon atoms into a plasma. Vapor growth method which uses Fe, Co, and Ni particles as catalysts and carbon ion bombardment of carbon whiskers [31] are other possible methods in synthesizing CNTs.

Chapter 3

Theoretical Background

Understanding the physical and chemical properties of matter in any phase and in any form is a complicated and advanced problem. In all cases the system is tried to be described by a number of nuclei and electrons interacting through electrostatic interactions. In principle all the properties can be derived by solving the many-body Schrödinger equation:

$$\widehat{H}\Psi_i(\mathbf{r},\mathbf{R}) = E_i\Psi_i(\mathbf{r},\mathbf{R}) \tag{3.1}$$

The Hamiltonian of a many body system can be written in a general form , like:

$$H = \sum_{I=1}^{N} \frac{\overrightarrow{P_I^2}}{2M_I} + \sum_{i=1}^{N_e} \frac{\overrightarrow{p_i^2}}{2m} + \sum_{i>j} \frac{e^2}{|\overrightarrow{r_i} - \overrightarrow{r_j}|} + \sum_{I>J} \frac{Z_I Z_J e^2}{|\overrightarrow{R_I} - \overrightarrow{R_J}|} - \sum_{i,I} \frac{Z_I e^2}{|\overrightarrow{R_I} - \overrightarrow{r_i}|} \tag{3.2}$$

where $R = R_I$, $I = 1...N$, symbolizes N nuclear coordinates, and $r = r_i$, $i = 1...N_e$, are considered to be N_e electronic coordinates. Z_I's are the nuclear charges and M_I's are the mass of Ith nuclei.

Clearly, it is almost impossible to solve this problem exactly except for a few simple cases. This is a many-body system described by second order, many component differential Schrödinger equation. One have to deal with $(3N_e + 3N)$ degrees of freedom to obtain a desired solution. Schrödinger equation cannot be easily decoupled into a set of independent equations because of electrostatic correlations between each component. To achieve the solution of this complex equation approximation methods have to be introduced.

3.1 Born-Oppenheimer Approximation

Due to the small mass of electrons compared with mass of the nuclei, electrons move much faster. Thus electrons have the ability to follow the motion of the nuclei instantaneously, so they remain in the stationary state of the electronic Hamiltonian set by the instanteneous nuclear configuration [32]. With these conditions, wave function can be factorized as follows:

$$\Psi(\mathbf{R},\mathbf{r},\mathbf{t}) = \Theta(\mathbf{R},t)\Phi(\mathbf{R},\mathbf{r}) \tag{3.3}$$

where nuclear wave function $\Theta(\mathbf{R},t)$ obeys the time-dependent Schrödinger equation and electronic wave function $\Phi(\mathbf{R},\mathbf{r})$ is the m-th stationary state of the electronic Hamiltonian. In spite of m can be any electronic eigenstate, in principle, most of the cases consider m=0 or in other words ground state corresponding to the equilibrium configuration of R.

On the other hand when the inter-atomic distances are larger than the thermal wavelength, and the potential energy surfaces in bonding environments are rigid enough to localize the nuclear wave functions, the solution of the nuclear equation is not necessary. In these cases nuclear wave packets are sufficiently localized and can be replaced by Dirac‘s δ-functions where the centers of these δ-functions are the classical positions, R^{cl}. The connection between quantum and classical mechanics can be achieved through Ehrenfest‘s theorem which considers the mean values of the position and momentum operators [33].

Assuming these approximations, we are left with the problem of solving the many-body electronic Schrödinger equation for fixed nuclear positions, generally corresponding to the equilibrium configuration of ions.

3.2 The Electronic Problem

Many-body electronic Schrödinger equation is still a very difficult problem to handle and exact solution is known only for some simple cases, such as free electron gas. At analytic level, one has to refer approximations.

In the early days of quantum mechanics (in 1928) first approximation method was proposed by Hartree[34]. It postulates that many-electron wave function can be written as product of one-electron wave functions each of which satisfies one-particle Schrödinger equation in an effective potential.

$$\Phi(\mathbf{R},\mathbf{r}) = \Pi_i \varphi(\mathbf{r}_i) \tag{3.4}$$

$$(-\frac{\hbar^2}{2m}\nabla^2 + V_{eff}^{(i)}(\mathbf{R},\mathbf{r}))\varphi_i(\mathbf{r}) = \epsilon_i \varphi_i(\mathbf{r}) \tag{3.5}$$

with

$$V_{eff}^{(i)}(\mathbf{R},\mathbf{r}) = V_n(\mathbf{R},\mathbf{r}) + \int \frac{\sum_{j\neq i}^{N} \rho_j(\mathbf{r'})}{|\mathbf{r}-\mathbf{r'}|} d\mathbf{r'} \tag{3.6}$$

where

$$\rho_j(\mathbf{r}) = e|\phi_j(\mathbf{r})|^2 \tag{3.7}$$

is the electronic density associated with particle j. Effective potential does not include the charge density terms associated with i, in order to prevent self-interaction terms. Here $V_n(\mathbf{R},\mathbf{r})$. In this approximation, the energy is given by:

$$E^H = \sum_i^N \varepsilon_n - \frac{1}{2}\int\int \frac{\rho(\mathbf{r})\rho(\mathbf{r'})}{|\mathbf{r}-\mathbf{r'}|} d\mathbf{r} d\mathbf{r'} \tag{3.8}$$

where the factor $1/2$ comes from the fact that electron-electron interaction is counted twice and $\rho(\mathbf{r})$ is defined as:

$$\rho(\mathbf{r}) = e\sum_j^{occ} \rho_j(\mathbf{r}) \tag{3.9}$$

The coupled differential equations in Eq. 3.5 can be solved by minimizing the energy with respect to a set of variational parameters in a trial wave function and then putting them back into Eq. 3.6, and solving the Schrödinger equation again. This procedure, which is called self-consistent Hartree approximation, should be repeated until the self-consistency is reached.

To improve Hartree approximation, fermionic nature of electrons should be considered. Due to Pauli exclusion principle, two fermions, electrons in our case, cannot occupy the same state being all of their quantum numbers are the same.

This suggests that total electron wave function should be in a antisymmetric form:

$$\Phi(\mathbf{R},\mathbf{r}) = \frac{1}{\sqrt{N!}} \begin{pmatrix} \phi_1(\mathbf{r_1}) & \dots & \phi_1(\mathbf{r_N}) \\ \vdots & \ddots & \vdots \\ \phi_N(\mathbf{r_1}) & \dots & \phi_N(\mathbf{r_N}) \end{pmatrix} \tag{3.10}$$

which is known as Slater determinant. This approximation is called Hartree-Fock-Slater (HFS) and it explains particle exchange in an exact manner [35, 65]. It also provides a moderate description of inter-atomic bonding, but many-body correlations of two electrons with opposite spins are completely absent. The correction of parallel spins are described partially by Fermi hole. Recently, the HFS approximation is routinely used as a starting point for more advanced calculations.

Parallel to the development in electronic theory, Thomas and Fermi proposed, at about same time as Hartree, that the full electron density was the fundamental variable of the many-body problem, and derived a differential equation for the density without referring to one-electron orbitals. Although, this theory which known as Thomas-Fermi Theory [37, 38], did not include exchange and correlation effects and was able to deal with bound states. It set up the basis of later development of Density Functional Theory (DFT).

3.3 Density Functional Theory

The initial work on DFT was reported in two publications: first by Hohenberg-Kohn in 1964 [39], and the next by Kohn-Sham in 1965 [40]. This was almost 40 years after Schrödinger (1926) had published his pioneering paper marking the beginning of wave mechanics. Shortly after Schrödinger‘s equation for electronic wave function, Dirac declared that chemistry had come to an end since all its content was entirely contained in that powerful equation. Unfortunately in almost all cases except for the simple systems like He or H, this equation was too complex to allow a solution. DFT is an alternative approach to the theory of electronic structure, in which the electron density distribution $\rho(\mathbf{r})$ rather than

many-electron wave function plays a central role. In the spirit of Thomas-Fermi theory [37, 38], it is suggested that a knowledge of the ground state density of $\rho(\mathbf{r})$ for any electronic system uniquely determines the system.

3.3.1 Hohenberg-Kohn Formulation

The Hohenberg-Kohn [39] formulation of DFT can be explained by two theorems:

Theorem 1: The external potential is univocally determined by the electronic density, except for a trivial additive constant.

Since $\rho(\mathbf{r})$ determines V($\mathbf{r}$), then it also determines the ground state wave function and gives us the full Hamiltonian for the electronic system. Hence $\rho(\mathbf{r})$ determines implicitly all properties derivable from the electronic Hamiltonian through the solution of the time-dependent Schrödinger equation.

Theorem 2: (Variational Principle) The minimal principle can be formulated in terms of trial charge densities, instead of trial wavefunctions.

The ground state energy E could be obtained by solving the Schrödinger equation directly or from the Rayleigh-Ritz minimal principle:

$$E = min\frac{\langle\widetilde{\Psi}|H|\widetilde{\Psi}\rangle}{\langle\widetilde{\Psi}|\widetilde{\Psi}\rangle} \tag{3.11}$$

Using $\widetilde{\rho}(\mathbf{r})$ instead of $\widetilde{\Psi}(\mathbf{r})$ was first presented in Hohenberg and Kohn. For a non-degenerate ground state, the minimum is attained when $\widetilde{\rho}(\mathbf{r})$ corresponds to a correct ground state density. And energy is given by the equation:

$$E_V[\widetilde{\rho}] = F[\widetilde{\rho}] + \int \widetilde{\rho}(\mathbf{r})V(\mathbf{r})d\mathbf{r} \tag{3.12}$$

with

$$F[\widetilde{\rho}] = \langle\Psi[\widetilde{\rho}]|\widehat{T} + \widehat{U}|\Psi[\widetilde{\rho}]\rangle \tag{3.13}$$

and $F[\widetilde{\rho}]$ requires no explicit knowledge of V($\mathbf{r}$).

These two theorems form the basis of the DFT. The main remaining error

is due to inadequate representation of kinetic energy and it will be cured by representing Kohn-Sham equations.

3.3.2 Kohn-Sham Equations

There is a problem with the expression of the kinetic energy in terms of the electronic density. The only expression used until now is the one proposed by Thomas-Fermi, which is local in the density so it does not reflect the short-ranged, non-local character of kinetic energy operator. In 1965, W. Kohn and L. Sham [40] proposed the idea of replacing the kinetic energy of the interacting electrons with that of an equivalent non-interacting system. With this assumption density can be written as

$$\rho(\mathbf{r}) = \sum_{s=1}^{2}\sum_{i=1}^{N_s} |\varphi_{i,s}(\mathbf{r})|^2 \tag{3.14}$$

$$T[\rho] = \sum_{s=1}^{2}\sum_{i=1}^{N_s} \langle\varphi_{i,s}| -\frac{\nabla^2}{2}|\varphi_{i,s}\rangle \tag{3.15}$$

where $\varphi_{i,s}$'s are the single particle orbitals which are also the lowest order eigenfunctions of Hamiltonian non-interacting system

$$\{-\frac{\nabla^2}{2} + v(\mathbf{r})\}\varphi_{i,s}(\mathbf{r}) = \epsilon_{i,s}\varphi_{i,s}(\mathbf{r}) \tag{3.16}$$

Using new form of $T[\rho]$ density functional takes the form

$$F[\rho] = T[\rho] + \frac{1}{2}\int\int \frac{\rho(\mathbf{r})\rho(\mathbf{r}')}{|\mathbf{r}-\mathbf{r}'|}d\mathbf{r}d\mathbf{r}' + E_{XC}[\rho] \tag{3.17}$$

where this equation defines the exchange and correlation energy as a functional of the density. Using this functional in 3.12, we finally obtain the total energy functional which is known as Kohn-Sham functional [40]

$$E_{KS}[\rho] = T[\rho] + \int \rho(\mathbf{r})v(\mathbf{r})d\mathbf{r} + \frac{1}{2}\int\int \frac{\rho(\mathbf{r})\rho(\mathbf{r}')}{|\mathbf{r}-\mathbf{r}'|}d\mathbf{r}d\mathbf{r}' + E_{XC}[\rho] \tag{3.18}$$

in this way we have expressed the density functional in terms of Kohn-Sham(KS) orbitals which minimize the kinetic energy under the fixed density constraint. In principle these orbitals are a mathematical object constructed in order to render

the problem more tractable, and do not have a sense by themselves. The solution of KS equations has to be obtained by an iterative procedure, in the same way of Hartree and Hartree-Fock equations.

3.4 Exchange and Correlation

3.4.1 Local Density Approximation (LDA)

The local density approximation [41] has been the most widely used approximation to handle exchange correlation energy. Its philosophy was already present in Thomas-Fermi theory but it was first presented by Kohn-Sham. The main idea of LDA is to consider the general inhomogeneous electronic systems as locally homogeneous and then use the exchange correlation corresponding to the homogeneous electron gas.

LDA favors more homogeneous systems. It over-binds molecules and solids but the chemical trends are usually correct.

3.4.2 Generalized Gradient Approximation (GGA)

Once the extent of the approximations involved in the LDA has been understood, one can start constructing better approximations. The most popular approach is to introduce semi-locally the inhomogeneties of the density, by expanding $E_{XC}[\rho]$ as a series in terms of the density and its gradients. This approximation is known as GGA [42] and its basic idea is to express the exchange-correlation energy in the following form:

$$E_{XC}[\rho] = \int \rho(\mathbf{r})\epsilon_{XC}[\rho(\mathbf{r})]d\mathbf{r} + \int F_{XC}[\rho(\mathbf{r}, \nabla\rho(\mathbf{r}))]d\mathbf{r} \tag{3.19}$$

where the function F_{XC} is asked to satisfy the formal conditions.

GGA approximation improves binding energies, atomic energies, bond lengths and bond angles when compared the ones obtained by LDA.

3.5 Implementation of Periodicity in Numerical Calculations

By using the represented formalisms observables of many-body systems can be transformed into single particle equivalents. However, there still remains two difficulties: A wave function must be calculated for each of the electrons in the system and the basis set required to expand each wave function is infinite since they extend over the entire solid. For periodic systems both problems can be handled by Bloch‘s theorem [43].

3.5.1 Bloch‘s Theorem

Bloch theorem states that in a periodic solid each electronic wave function can be written as:

$$\Psi_i(\mathbf{r}) = u_i(\mathbf{r})e^{i\mathbf{kr}} \tag{3.20}$$

where u_k has the period of crystal lattice with $u_k(\mathbf{r}) = u_k(\mathbf{r}+\mathbf{T})$. This part can be expanded using a basis set consisting of reciprocal lattice vectors of the crystal.

$$u_i(\mathbf{r}) = \sum_G a_{k,G} e^{i(\mathbf{G})\mathbf{r}} \tag{3.21}$$

Therefore each electronic wave function can be written as a sum of plane waves

$$\Psi_i(\mathbf{r}) = \sum_G a_{i,k+G} e^{i(\mathbf{k}+\mathbf{G})\mathbf{r}} \tag{3.22}$$

3.5.2 k-point Sampling

Electronic states are only allowed at a set of **k**-points determined by boundary conditions. The density of allowed **k**-points are proportional to the volume of the cell. The occupied states at each **k**-point contribute to the electronic potential in the bulk solid, so that in principle, a finite number of calculations are needed to compute this potential. However, the electronic wave functions at **k**-points

that are very close to each other, will be almost identical. Hence, a single **k**-point will be sufficient to represent the wave functions over a particular region of **k**-space. There are several methods which calculate the electronic states at special **k**-points in the Brillouin zone [44]. Using these methods one can obtain an accurate approximation for the electronic potential and total energy at a small number of **k**-points. The magnitude of any error can be reduced by using a denser set **k**-points.

3.5.3 Plane-wave Basis Sets

According to Bloch's theorem, the electronic wave functions at each **k**-point can be extended in terms of a discrete plane-wave basis set. Infinite number of plane-waves are needed to perform such expansion. However, the coefficients for the plane waves with small kinetic energy $(\hbar^2/2m)|\mathbf{k}+\mathbf{G}|^2$ are more important than those with large kinetic energy. Thus some particular cutoff energy can be determined to include finite number of **k**-points. The truncation of the plane-wave basis set at a finite cutoff energy will lead to an error in computed energy. However, by increasing the cutoff energy the magnitude of the error can be reduced. the selection of an appropriate cut-off energy depends on the pseudoptential of the ions, and determined by convergence tests.

When plane waves are used as a basis set, the Kohn-Sham(KS) [40] equations assume a particularly simple form. In this form, the kinetic energy is diagonal and potentials are described in terms of their Fourier transforms. Solution proceeds by diagonalization of the Hamiltonian matrix. The size of the matrix is determined by the choice of cutoff energy, and will be very large for systems that contain both valence and core electrons. This is a severe problem, but it can be overcome by considering pseudopotential approximation.

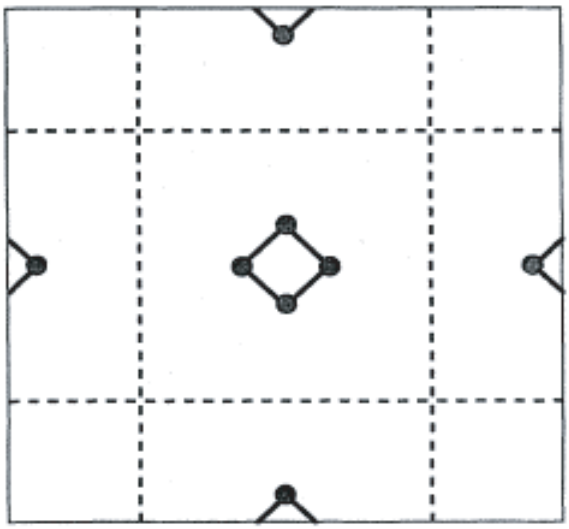

Figure 3.1: A schematic description of supercell geometry for a hypothetical square molecule. Supercell is chosen large enough to prevent interactions between the molecules.

3.5.4 Supercell Geometry

The Bloch Theorem cannot be applied to a non-periodic systems, such as a system with a single defect. A continuous plane-wave basis set would be required to solve such systems. Calculations using plane-wave basis sets can only be performed on these systems if a periodic supercell is used. Periodic boundary conditions are applied to supercell so that the supercell is reproduced through out the space. As seen schematically in Fig. 3.1 even molecules can be studied by constructing a supercell which is large enough to prevent interactions between molecules.

3.6 Pseudopotential Approximation

It is well-known that most physical properties of solids are dependent on the valence electrons to a much greater extent than on the core electrons. The pseudoptential approximation utilizes this idea by replacing the core electrons and the

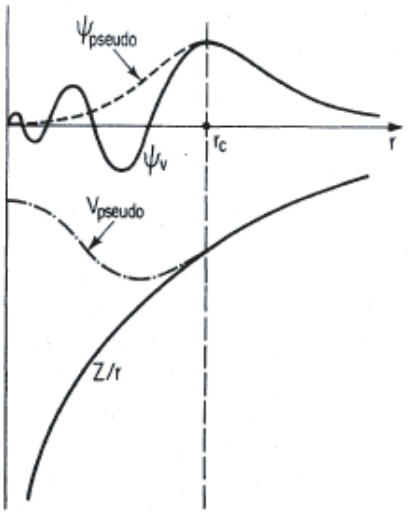

Figure 3.2: Illustration of all-electron (solid lines) and pseudoelectron (dashed lines) potentials and their corresponding wave functions.

strong ionic potential by a weaker pseudopotential that acts on a set of pseudo wave functions rather than the true valence wave functions. An ionic potential, valence wave function and corresponding pseudopotential and pseudo wave function are illustrated in Fig. 3.2.

Chapter 4

Results

Single-wall carbon nanotubes[6, 7] (SWNT) can be functionalized by adsorption of atoms or molecules, which can induce dramatic changes in the physical and chemical properties of the bare tube. Functionalization of SWNTs has been attracting our interest for two possible, insofar technologically important applications; namely fabrication of metallic nanowires and nanomagnets. As nanoelectronics are promising rapid miniaturization providing higher and higher device density and operation speeds, the fabrication of interconnects with high conductance and low energy dissipation appear to be real technological problems. Since the first day of molecular electronics, which was proposed as a future direction in microelectronics, the interconnects and contacts to individual molecular devices have remained a real challenge.

Very thin metal wires and atomic chains were produced by retracting the STM tip from an indentation and then by thinning the neck of the materials that wets the tip[45, 46, 47]. While those nanowires produced so far played a crucial role in understanding the quantum effects in electronic and thermal conductance[48, 49, 50, 51, 52], they were neither stable nor reproducible to offer any relevant technological application. Nowadays, the most practical and realizable method to fabricate nanowires seems to rely on carbon nanotubes.

Earlier experimental studies have indicated that SWNTs can serve as templates to produce reproducible, very thin metallic wires with controllable sizes[53]. These metallic nanowires can be used as conducting connects and hence are important in nanodevices based on molecular electronics. Recently, Zhang et al[26]. have shown that continuous Ti coating of varying thickness, and quasi continuous coating of Ni and Pd can be obtained by using electron beam evaporation techniques. However, metal atoms such as Au, Al, Fe, Pb were able to form only isolated discrete particles or clusters instead of a continuous coating of SWNT.

Not only metallic connects, but also the contacts of metal electrodes themselves are crucial for the operation of devices based on nanotubes. Low resistance ohmic contacts to metallic and semiconducting SWNTs were achieved by Ti and Ni[25]. The formation of Schottky barrier at the contact has been found to be responsible for the operation of field emission transistors made from SWNTs[19, 54, 55].

Theoretical studies [56] have indicated that stable rings and tubes of Al atoms can form around a semiconducting SWNT. It is argued that either persistent currents through these conducting nanorings, or conversely very high magnetic fields can be induced at their center[56]. Such a set-up has been also proposed as possible qubits in quantum computation[57].It has been shown experimentally that the implementation of iron atoms inside the tube can give rise to magnetization[58]. Such a system may be specified as nanomagnet, and can be used in several applications ranging from various research tools to high density storage devices.

As a second motivation of our study, we expect that novel molecular nanomagnets and electromagnetic devices can be generated from these nanostructures formed by the adsorption of specific atoms on the surface of SWNTs according to a given pattern. Thus, the study of adsorption of atoms on nanotube surfaces is essential to achieve low resistance ohmic contacts to nanotubes, to produce nanowires with controllable size, and to fabricate nanomagnets and functional nanodevices.

This thesis presents an extensive study of the adsorption of individual atoms on the surface of a semiconducting (8,0) and also a metallic (6,6) SWNT. The

binding geometry and binding energy and resulting electronic structure of various (ranging from alkali and simple metals to group IV elements, and including most of the transition metal) atoms have been investigated. Our prime objective is to reveal the character and geometry of the bonding, and to understand why some metal atoms form strong bonds while others are only weakly bound. The effect of the adsorption on the physical properties, such as electronic, magnetic, is another issue, which we deal in detail in this work. Specifically, we addressed the question whether the ground state of a SWNT with an adsorbed atom has a net spin. We have explored the situation whether the magnetic ground state gives rise to the bands with one type of spin. Finally, we discuss the subject of connecting the SWNTs and hence making networks by carbon adatoms. We believe that our results are important for a number of applied and theoretical research, such as coating of carbon nanotubes [16], design and fabrication of functionalized nanodevices and nanomagnets; spintronics; gluing SWNTs to generate cross-bar, T, Y etc. structures; and forming metal-SWNT junctions and contacts.

4.1 Method of calculations

Our study deals with the adsorption of 27 different single atoms on the (8,0) zigzag SWNT, and four different atoms on the (6,6) armchair SWNT. The atomic structure, binding geometry and binding energy, and resulting electronic structure of an individual atom adsorbed SWNTs have been calculated by using a first-principles pseudopotential plane wave method within the generalized gradient approximation (GGA) [60]. Earlier, the first-principle pseudopotential method using supercell method has been demonstrated to provide accurate predictions on the mechanical and electronic properties of various zigzag and armchair SWNTs for undeformed and radially deformed cases[59, 61, 62].

Spin-unpolarized and spin-polarized (relaxed) calculations have been carried out for single atom, bare SWNT, and single atom absorbed SWNT [13, 14]. Ultra soft pseudopotentials [63] and plane waves up to an energy cutoff of 300 eV

depending on the pseudopotential are used. The Brillouin zone of the supercell is sampled by (1,1,11) **k**-points within the Monkhorst-Pack special **k**–point scheme[44]. Calculations have been performed in momentum space by using periodically repeating tetragonal supercell with lattice constants, $a_s = b_s \sim 15$ Å and c_s. To minimize the adsorbate-adsorbate interaction, the lattice constant along the axis of the tube, c_s, is taken to be twice the 1D lattice parameter of the bare tube, *i.e.* $c_s \sim 2c$ for the zigzag SWNT and $c_s \sim 4c$ for the armchair SWNT.

For the adsorption of individual atoms we considered four possible sites (*i.e.* H-site, above the hexagon; Z-, and A-sites above the zigzag and axial C-C bonds; and T-site above the carbon atom) as described in Fig. 4.1. The binding sites are determined by optimizing all atomic positions (adsorbate atom and 64 carbon atoms of the (8,0) SWNT or 96 carbon atoms of the (6,6) SWNT, as well as c_s(hence c) using the conjugate gradient (CG) method. Binding energies are obtained from the expression,

$$E_b^{u(p)} = E_T^{u(p)}[SWNT] + E_T^{u(p)}[A] - E_T^{u(p)}[A + SWNT] \tag{4.1}$$

in terms of the total energies corresponding to the fully optimized structure of bare nanotube ($E_T^{u(p)}[SWNT]$), free atom A ($E_T^{u(p)}[A]$), and the atom A adsorbed on a SWNT ($E_T^{u(p)}[A+SWNT]$). The superscript $u(p)$ indicates spin-unpolarized (spin-polarized) energies. The binding energies $E_b^{u(p)}$ are obtained from the total energies corresponding to either non-magnetic (spin-unpolarized) state with zero net spin or magnetic (spin-relaxed) state with net spin. A bare nanotube has a non-magnetic ground state with zero net spin. $E_b^{u(p)} > 0$ corresponds to a CG optimized stable structure and indicates the bonding (a local or global minimum on the Born-Oppenheimer surface). Only the short range (chemical) interactions are included in the binding energy, $E_b^{u(p)}$. Long range Van der Waals interaction, E_{vdW} is expected to be much smaller than the chemisorption binding energy and is omitted. However, for specific elements, such as Mg, Zn, the binding energy is small and the character of the bond is between chemisorption and physisorption. In this case, the weak and attractive Van der Waals interaction energy becomes crucial. It can be calculated from the asymptotic form of the

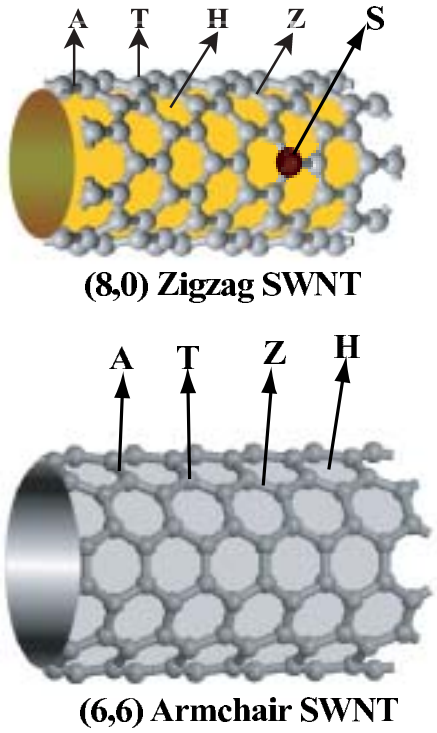

Figure 4.1: A schematic description of different binding sites of individual atoms adsorbed on a zigzag (8,0) and armchair (6,6) tubes. H: hollow; A: axial; Z: zigzag; T: top; S: substitution sites.

Lifshitz's formula[64], $E_{vdW} = \sum_{ij} C_{6ij}/r_{ij}^6$ with the coefficients C_{6ij} are obtained from the Slater-Kirkwood approximation[65]. We note that the asymptotic form of E_{vdW} may not be accurate when adatom-SWNT distance is small.

4.2 Binding geometry and binding energy

The cohesive energies of C atoms in the (8,0) and (6,6) tube, *i.e.* $E_c = (NE_T^u[C] - E_T^u[SWNT])/N$, (N being the number of C atoms in the unit cell of SWNT) are calculated to be $E_c^{(8,0)}$ =9.06 eV and $E_c^{(6,6)}$ =9.14 eV, respectively. The zigzag (8,0) SWNT is an insulator with a calculated band gap, E_g =0.64 eV. The (6,6)

armchair SWNT is a metal, since π^*-conduction and π-valence bands cross at the Fermi level. As far as the electronic properties are concerned, our study has sampled two extreme cases in the class of SWNTs. The binding geometries and binding energies E_b^u, calculated from spin-unpolarized total energies as Eq. 4.1 are given in Table 4.1 for the (8,0) SWNT and in Table 4.2 for the (6,6) SWNT.

The interaction between SWNT and most of the adatoms considered in this study is significant and results in chemisorption bond. Thus, the binding energy corresponding to a non-magnetic state ranges from $\sim$ 1 eV to $\sim$4.5 eV. While alkali and simple metals have binding energy in the range of 1.5 eV, the chemisorption energy of transition metals is relatively higher. On the other hand, metals like Cu, Au, Ag and Zn have relatively weak binding. The attractive Van der Waals interaction may be important for their stabilization. The Group IV elements, such as C and Si, can also be bound with a significant binding energy. The center of the hexagons (i.e. H-site) made by C-C-C bonds on the SWNT surface appears to be favored by most of the adatoms. The average C-adatom bond distance occurs in the range of 2.0-2.3 Å. However, $\bar{d}_{C-A}$ is relatively smaller for H, C, O atoms having small atomic radii. It is well known that the interaction between the graphite surface and most of the atoms included in Table 4.1 and Table 4.2 is actually weak. The curvature effect is the primary factor that strengthens the binding.[61]

We note that specific adsorbate-SWNT (A+SWNT) systems are found to be in a magnetic ground state, hence $E_T^p[A+SWNT] < E_T^u[A+SWNT]$. No matter what the value of the binding energy is, a stable binding of a particular A+SWNT geometry is meaningful if it belongs to a ground state. In Table 4.3 and Table 4.4 we present the differences between the spin-unpolarized and spin-polarized total energies, *i.e.* $\Delta E_T = E_T^u[A+SWCT] - E_T^p[A+SWNT]$. Here $\Delta E_T > 0$ indicates that magnetic ground state with a net spin is favored. This table is crucial for the further study coverage of SWNTs with foreign atoms (Sc, Co, Ti, Nb, Ta) to generate magnetic nanostructure.

We can extract following useful information from the results of calculations listed in these Tables. In general, the binding energies calculated for non-magnetic

Table 4.1: Calculated binding energies and average carbon-adatom bond distances, $\bar{d}_{C-A}$ of individual atoms adsorbed at H-, Z-, A-, and T-sites of the (8,0) SWNT as described in Fig. 4.1. Binding energies, E_b^u are obtained from spin-unpolarized total energies calculated for fully relaxed atomic structure. Results for hydrogen and oxygen atoms are taken from Refs. [59, 15]. →H implies that the adatom at the given site is not stable and eventually it moves to the H-site.

Atom	H (eV)	A (eV)	Z (eV)	T (eV)	d_{C-A} (A^o)
Na	1.3	1.1	1.1	1.1	2.3
Mg	0.08	0.07	0.05	0.07	3.8
Sc	2.1	1.4	1.5	→ H	2.3
Ti	2.9	2.1	2.7	2.1	2.2
V	3.2	2.2	→ H	→ H	2.1
Cr	3.7	2.5	→ H	→ H	2.0
Mn	3.4	2.5	→ H	→ H	2.1
Fe	3.0	2.5	→ H	1.6	2.1
Co	2.8	2.5	→ H	→ H	2.1
Ni	2.2	2.4	2.3	→ A	1.9
Cu	0.5	0.8	0.6	→ A	2.1
Zn	0.05	0.05	0.03	0.04	3.7
Nb	3.9	2.7	→ H	→ H	2.2
Mo	4.6	3.0	→ H	→ H	2.2
Pd	1.1	1.6	1.5	1.5	2.1
Ag	0.1	0.3	→ A	→ A	2.7
Ta	2.8	2.4	2.5	→ H	2.1
W	3.4	2.5	2.6	3.3	2.1
Pt	→ Z	2.7	2.4	→ A	2.1
Au	0.3	0.6	0.4	0.6	2.2
Al	1.6	1.4	1.5	→ H	2.3
C	→ Z	3.7	4.2	→ A	1.5
Si	2.5	2.2	2.5	2.2	2.1
Pb	1.3	1.0	1.2	→ H	2.6
S	→ A	2.8	2.4	→ Z	1.9

Table 4.2: Calculated binding energies and average carbon-adatom bond distances, $\bar{d}_{C-A}$ of individual atoms adsorbed at H-, Z-, A-, and T-sites of the (6,6) SWNT as described in Fig. 4.1. Binding energies, E_b^u are obtained from spin-unpolarized total energies calculated for fully relaxed atomic structure.

Atom	H (eV)	A (eV)	Z (eV)	T (eV)	d_{C-A} (A^o)
Ti	2.62	1.66	1.79	1.74	2.2
Mn	3.25	→ H	→ H	→ H	2.1
Mo	4.34	→ H	→ H	→ H	2.2
Au	0.23	0.27	→ T	0.41	2.3

state are higher than those corresponding to the magnetic ground state. This is partly due to the reference of energies in Eq. 4.1. Most of the transition metal atoms adsorbed on the (8,0) and (6,6) SWNT have magnetic ground state with $\Delta E_T > 0$, and hence they give rise to the net magnetic moment ranging from $5.49\mu_B$ (for Mn) to zero magnetic moment (for Pd and Pt). While Ni adsorbed SWNT has very low magnetic moment ($0.04\mu_B$), the adsorbates such as Au, Ag or Cu have magnetic moment in the range of $0.4 - 0.6\mu_B$. Our spin-polarized and spin-unpolarized calculations show that these transition metal atoms in Table 4.3 have also magnetic ground state when they are free. Since a bare SWNT having a non-magnetic ground state, the net spin of the A+SWNT system originates from the magnetic moment of the adsorbed atom. The calculated magnetic moments of these free atoms are in good agreement with the values given by Moore[66]. On the other hand, atoms, such as Na, Al, C, Si, Pb, O, S, H, favor non-magnetic ground state when adsorbed on the (8,0) SWNT. The magnetic moment generated upon the adsorption of individual transition atoms has important implications, and points to an issue, whether molecular magnets (or nanomagnets) can be produced from carbon nanotubes. Addressing this issue may open an active field of study on SWNTs, which are covered or substitutionally doped by transition metal atoms according to a well-defined pattern. Implementation of transition metal elements inside the tube is another way to obtain nanomagnetic structures. This way, these atoms are prevented from oxidation. Whether a permanent magnetic moment by the exchange interaction can be generated on these transition metal coated SWNTs would be an interesting question to answer. Recently, the

Table 4.3: Strongest binding site (as described in Fig. 4.1); adsorbate-carbon distance $\bar{d}_{C-A}$; the difference between spin-unpolarized and spin-polarized total energies ΔE_T; binding energy E_b^u obtained from spin-unpolarized calculations; binding energy E_b^p obtained from spin-polarized calculations; magnetic moment (μ_B per supercell) of the magnetic ground state corresponding to the adsorption of various individual atoms on the (8,0) SWNT.

Atom	Site	$d_{C-A}(A^o)$	$\triangle E_T(eV)$	$E_b^u(eV)$	$E_b^p(eV)$	$\mu(\mu_B)$
Na	H	2.3	-	1.3	-	-
Mg	H	3.8	-	0.08	-	-
Sc	H	2.2	0.15	2.1	1.9	0.64
Ti	H	2.2	0.58	2.9	2.2	2.21
V	H	2.2	1.20	3.2	1.4	3.67
Cr	H	2.3	2.25	3.7	0.4	5.17
Mn	H	2.4	2.42	3.4	0.4	5.49
Fe	H	2.3	1.14	3.1	0.8	2.27
Co	H	2.0	0.41	2.8	1.7	1.05
Ni	A	1.9	0.02	2.4	1.7	0.04
Cu	A	2.1	0.03	0.8	0.7	0.53
Zn	H	3.7	0	0.05	0.04	0
Nb	H	2.2	0.40	3.9	1.8	2.86
Mo	H	2.2	0.32	4.6	0.4	4
Pd	A	2.1	0	1.7	1.7	0
Ag	A	2.5	0.03	0.3	0.2	0.6
Ta	H	2.2	0.73	2.9	2.4	3.01
W	H-A	2.1	0.59	3.4	0.9	2.01
Pt	A	2.1	0	2.7	2.4	0
Au	A-T	2.2	0.04	0.6	0.5	1.02
Al	H	2.3	-	1.6	-	-
C	Z	1.5	-	4.2	-	-
Si	H	2.1	-	2.5	-	-
Pb	H	2.6	0.01	1.3	0.8	0
H	T	1.1	-	2.5	-	-
O	Z	1.5	-	5.1	-	-
S	A	1.9	-	2.8	-	-

Table 4.4: Strongest binding site (as described in Fig. 4.1); adsorbate-carbon distance $\bar{d}_{C-A}$; the difference between spin-unpolarized and spin-polarized total energies ΔE_T; binding energy E_b^u obtained from spin-unpolarized calculations; binding energy E_b^p obtained from spin-polarized calculations; magnetic moment μ per supercell corresponding to the magnetic ground state corresponding to the adsorption of individual Ti, Mn, Mo, Au atoms on a (6,6) SWNT.

Atom	Site	$d_{C-A}(A^o)$	$\triangle E_T$(eV)	E_b^u(eV)	E_b^p(eV)	$\mu(\mu_B)$
Ti	H	2.2	0.48	2.62	1.81	1.68
Mn	H	2.5	2.23	3.25	0.1	5.60
Mo	H	2.3	0.2	4.34	0.1	3.61
Au	T	2.3	0.02	0.41	0.28	0.79

magnetization and hysteresis loops of iron nanoparticles partially encapsulated at the tips and inside of aligned carbon nanotubes have been demonstrated by recent experimental works.[58]

Figure. 4.2 presents the variation of the ground state properties[67] (such as the cohesive energy E_c and bulk modulus B), binding energies E_b^u and E_b^p of the first row transition metal elements with respect to the number of d-electrons N_d. $E_c(N_d)$ and $B(N_d)$ curves show a minimum (at $N_d = 5$ for the $3d^5 4s^2$ configuration of Mn atom) between two maxima of equal strength; first maximum occurs at $N_d = 3$ or 4, the second one at $N_d = 7$. This behavior of bulk properties were explained by the Friedel model[68]. Although the overall shape of the variation of the binding energies of first row transition metal atoms with N_d, $E_b^p(N_d)$, is reminiscent of the $B(N_d)$ and $E_c(N_d)$, there are some differences. The binding energy of Ti($N_d = 2$) is highest, and hence the first maximum is higher than the second one $E_b^p(N_d = 7)$ and $E_b^p(N_d = 8)$ corresponding to the binding energies of Co and Ni. While the binding energy of Sc(N_d=1) is close to that of Ti at the first maximum, the binding energy of Cu($N_d = 10$) is small, and it eventually decreases to almost zero for Zn, which has a filled valence shells (i.e $3d^{10}4s^2$). Interestingly, Cr and Mn atoms which have the same $3d^5 4s^2$ configuration, have similar binding energies forming the minimum between double maximum, but different E_c and B. The variation of E_b^u and E_b^p with N_d, however, shows dramatic differences. While $E_b^p(N_d)$ mimics $E_c(N_d)$ and has a minimum for N_d =5,

as E_c and B do, E_b^u passes through a maximum. This situation confirms that magnetic states correspond to ground state.

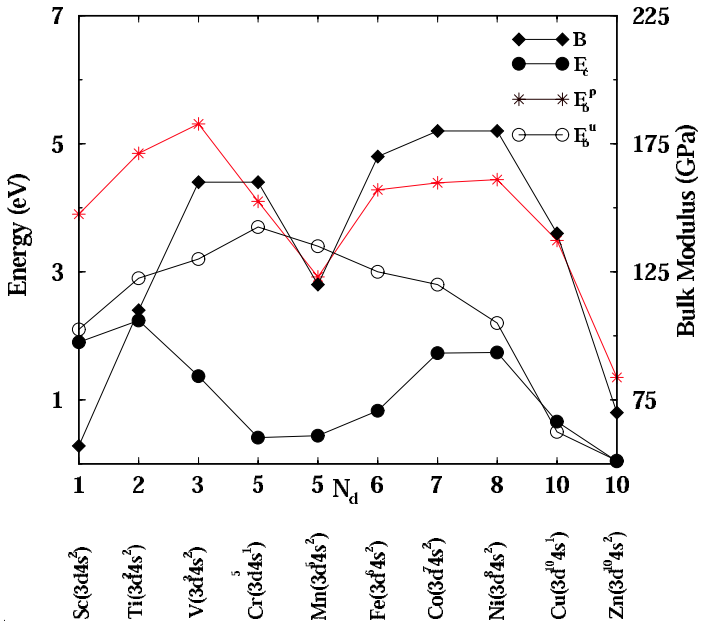

Figure 4.2: Variation of the calculated spin-unpolarized E_b^u and spin-polarized E_b^p binding energy of transition metal atoms with respect to the number of d-electrons N_d. The bulk cohesive energy E_c and the bulk modulus B from Ref [43]. is included for the comparison of the trends.

Binding energies listed in Table 4.3 are of particular interest for coating of SWNTs by metal atoms, and hence for the fabrication of nanowires. The atoms which were observed to form continuous and quasi continuous coating on the SWNT (Ti, Ni, and Pd) have relatively higher binding energies as compared to those atoms (Au, Fe, Pb) which form only discrete particles on the surface of the tube [53]. We also note that in forming a good coverage not only adatom-SWNT interaction, but also other factors, possibly adatom-adatom interaction play a crucial role. Good conductors such as Au, Ag, and Cu have very weak binding. On the other hand, Na with one 3s-electron on the outer shell is bound with a significant binding energy (E_b =1.3 eV). The binding energy of Mg is very weak and is only 0.03 eV at the H-site due to its outer shell $(3s)^2$. For the same reason Zn by itself exhibits the similar trend ($E_b^u = 0.05eV$) with its $(4s)^2$ valence structure. Owing to the weak binding the type of the bond

between Mg (Zn) and SWNT is between chemisorption and physisorption with $d_{C-A} = 3.8A^o (d_{C-A} = 3.7A^o)$. While an individual Al atom (with $(3s)^2 3p$-valence structure)is not bound to the graphite surface, its binding on the (8,0) SWNT is relatively strong . This can be explained by the curvature effect, since the binding was found to be even stronger at the high curvature site of SWNT under uniaxial radial deformation [61, 62]. Here we point out an interesting trend between Table 4.1 and Table 4.2, and also between Table 4.3 and Table 4.4. The binding energies E_b^u, as well as E_b^p and magnetic moments of the adatom adsorbed on the (8,0) SWNT came out to be consistently lower for the adatom adsorbed on the (6,6) tube. Perhaps, this trend can also be explained by the curvature effect[61, 69].

The transition metal atoms with a few d-electrons, such as Sc, Co, Ti, Nb, Ta form strong bonds with a binding energy ranging from 2.4 eV to 1.8 eV, and hence can be suitable for metal coating of SWNT. These metals can also be used as a buffer layer to form uniform coating of good conductors such as Au, Ag, Cu. Most of the adatoms we studied yield strongest binding at the H-site. Ni, Pd, Pt (column VIII elements) and Cu, Ag, Au (column I-B elements) seem to prefer A-site. The average adsorbate-C distance, $\bar{d}_{C-A}$, ranges between 1.9 Å (minimum) and 3.7 Å (maximum); most of them occur at ∼2.1 Å.

4.3 Interaction of Group IV elements with SWNT

The interaction of group IV elements with SWNT is crucial, since they have the same valence configuration. Here we consider parent C atom and Si. These atoms form rather strong bonds with the SWNT. The calculated binding energies of individual C and Si atoms are rather high, *i.e.* $E_b = 4.2$ and 2.5 eV, respectively. The Z-site is energetically favorable for both C and Si. The character of the bond will be clarified in Sec. V.

The substitution of Si is of particular interest, because SiC is a stable crystal.

The Si substitution can be realized by replacing one of the carbon atoms of the (8,0) SWNT by Si, and subsequently by relaxing carbon atoms and Si until practically zero force on all these atoms are achieved. To get an idea about the energetics of Si substitution we calculated the self-consistent total energies of two different systems. First system consisting of a (structure optimized) bare (8,0) SWNT and a single Si atom placed at the farthest point from the SWNT in the supercell has the total energy $E_T[SWNT, Si]$. Second system corresponding to a structure optimized, Si substituted SWNT and a single C atom placed at the farthest point has the total energy $E_T[SWNT(Si), C]$. The structure optimized Si substituted SWNT [SWNT(Si)] has found to be stable. The difference of energy, $\Delta E = E_T[SWNT(Si), C] - E_T[SWNT, Si]$, can give an idea about the energy involved in Si substitution. We found ΔE is positive ($\sim$6eV) and hence the substitution of Si is energetically unfavorable and corresponds to a local minimum in the Born-Oppenheimer surface. Following the definition by Baierle *et al.*[70] the substitution energy of a single Si *i.e.* $E_S = E_T[SWNT(Si)] - E_T[SWNT] - (\mu_{Si} + \mu_C)$, is calculated to be $E_S = 2.75$ eV by using the bulk cohesive energies of Si and C for μ_{Si} and μ_C respectively. This energy is comparable with the substitution energy of Si calculated for the (10,0) and (6,6) SWNT's[70]. If we use the adsorption energies of Si and C in Table 4.3 for μ_{Si} and μ_C, the formation energy is found to be 4.67 eV. This latter energy (E_S =4.67 eV) is closer to ΔE =6 eV than the previous energy (E_S =2.75) eV. Nevertheless, both substitution energies calculated by using different definitions indicate that the substitution of C in SWNT by Si is unfavorable energetically, hence it is endothermic.

The strong bond formation between C and SWNT suggests that two SWNTs can be connected by C adatoms. We examined the system of two parallel (8,0) SWNTs with a C atom placed at the mutual A-sites of these tubes. A system consisting of two parallel (8,0) SWNT connected by a C adatom in a supercell has been relaxed. The binding energy of the additional C atom connecting the tubes has been calculated from the following relation, $E_b = E_T[C] + E_T[SWNT, SWNT] - E_T[SWNT + C + SWNT]$, and found to be 4.6 eV. The atomic configuration and the local density of states (LDOS) of fully relaxed two SWNT connected by a C atom is shown in Fig. 4.3.

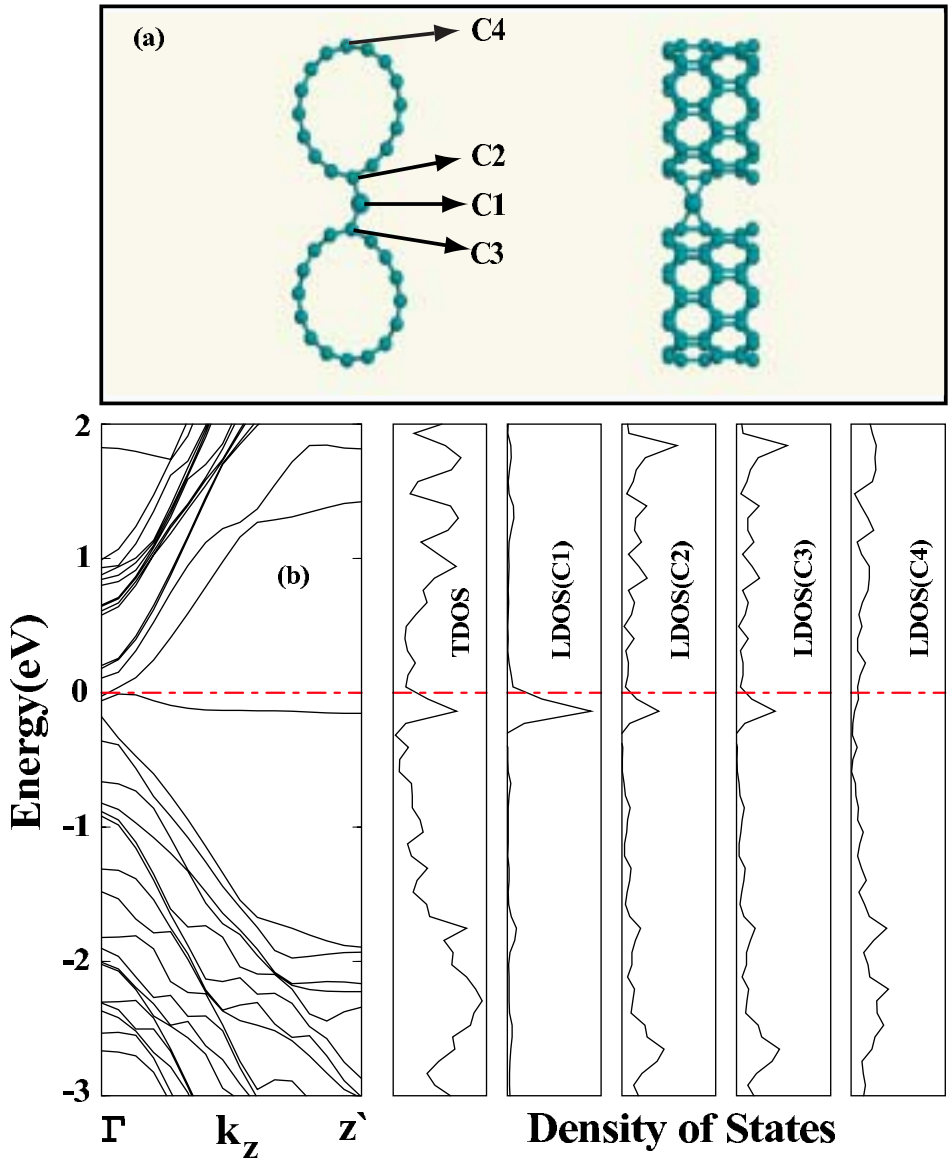

Figure 4.3: (a) Side views of atomic configuration of two (8,0) SWNT connected by a carbon adatom (per supercell) located at the mutual A-sites. C1, C2, C3, and C4 indicate specific atoms, where LDOS's are calculated. These are the connecting carbon adatom (C1), the C atoms (C2,C3) of SWNT which form bonds with C1, and the C atom of SWNT which is farthest from the region where two SWNTs are connected (C4). (b) The energy band structure. TDOS and LDOSs at C1, C2, C3, and C4. Zero of energy is taken at the Fermi level.

The carbon atom between the tubes form four directional bonds, two bonds to the C atoms of the C-C axial bonds of each SWNT. We note a slight deformation and deviation from circular cross section of SWNT, where the C adatom is attached. LDOS calculated at the connecting carbon adatom and at the carbon atoms of SWNTs shows a finite density of states at the Fermi level. A flat band derived from the C-C bonds overlaps with the lowest conduction band, and hence metallizes whole system as described in Fig. 4.3.

4.4 Character of the bond between adsorbed atom and SWNT

In this section the character of the bond between adatom and SWNT has been examined by the charge density analysis. For the fully relaxed, minimum total energy configuration we calculated the total and difference charge densities. The total charge density: $\rho(\mathbf{r}) = \sum_{n,k}^{occup} \Psi^*_{n,k}(\mathbf{r})\Psi_{n,k}(\mathbf{r})$, and the difference charge density: $\Delta\rho(\mathbf{r}) = \rho[A + SWNT] - \rho[SWNT] - \rho[A]$. In the latter equation the total charge densities of adatom adsorbed SWNT $\rho[A + SWNT]$, of bare SWNT $\rho[SWNT]$, and of free atom $\rho[A]$, all are calculated in the same supercell with the same atomic positions described in Eq. 4.1. Thereafter, the difference charge density conveys information about the charge rearrangements upon adsorption. In Fig. 4.4 we show $\rho(\mathbf{r})$ and $\Delta\rho(\mathbf{r})$ calculated for four adatoms, namely Na, Al, C, Ti. We did not present the counter plots of $\rho(\mathbf{r})$ for [Na + SWNT], since they do not convey relevant information owing to the low charge density around adsorbed Na atom. Dramatic differences in the valence electron configuration of these adatoms are reflected to the character of the bonds they form with SWNT.

Our analysis shows that charge is generally transferred from adatom and the C-C bond of SWNT. The $3s$ valence state of Na is weakly bound and is donated to the conduction band of the SWNT. Therefore, the band is modified. In the case of Al, which is adsorbed at the H-site, electrons are transferred from Al and nearest C atoms to the region between Al atom and the center of the hexagon on the surface of SWNT and to the C-C bond. The character of the bond formed

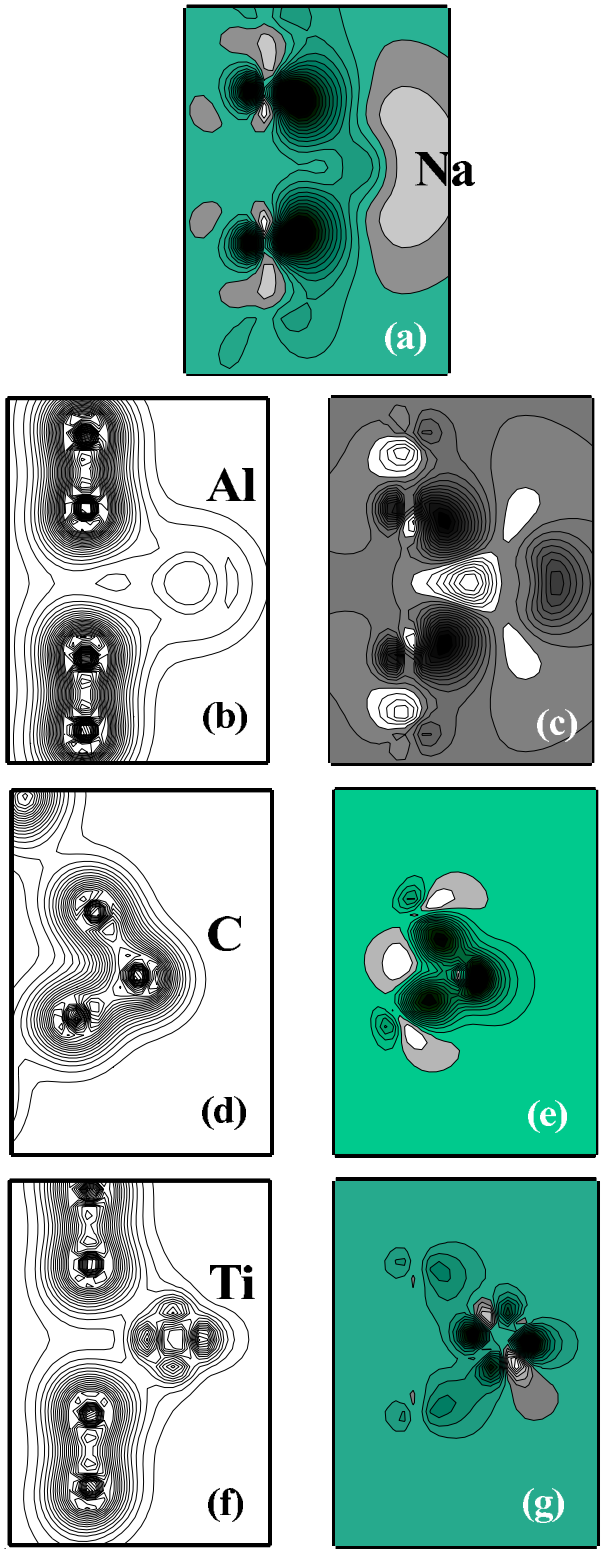

Figure 4.4: Contour plots of total $\rho(\mathbf{r})$ and difference $\Delta\rho(\mathbf{r})$ charge densities. For C the charge densities are calculated on a plane passing through adatom and zigzag C-C bond. For others (Na, Al, Ti) the charge density plane passes through the center of hexagon and adatom. In contour plots of $\Delta\rho(\mathbf{r})$, charge is depleted from black regions and is accumulated at white regions.

between adatom carbon and C atoms of SWNT is reminiscent of the sp^3 covalent bonds in diamond crystals. $\rho(\mathbf{r})$ has maximum value at the center of the C-C bonds. Because of new bond formation charge is transferred to the back bonds. The charge density of adsorbed Si exhibits a character similar to that of adsorbed C. Directional bonds form between Si and C atoms. Ti atom adsorbed at the H-site form a bond. The d-orbitals are responsible from this bond. According to the Mulliken analysis the transfer of charge from the Ti atom is 1.45 electrons for spin-unpolarized case. The interaction between Au atom and SWNT is weak, which results in a small binding energy. Accordingly, the charge rearrangement as result of Au adsorption is minute.

4.5 Electronic structure of adatom-SWNT system

Modification of electronic structure induced by the adsorbed foreign atoms is the prime interest of this study. We analyze the induced modifications by energy band structure and local and total density of states obtained for fully relaxed structures. An individual atom adsorbed on a SWNT may give rise to resonance states in the valence and conduction bands, and also localized states in the band gaps. Owing to the supercell method used in this study the energy states associated with a single adsorbate form energy bands, however. Actually these bands correspond to a linear chain of adsorbates with a 1D lattice constant c_s. The dispersion or width of the bands is a measure of the adsorbate-adsorbate coupling. To reduce the adsorbate-adsorbate coupling, which is a spurious effect of the supercell method, we have considered one adsorbate per two unit cell for the (8,0) zigzag SWNT (*i.e.* $c_s \sim 2c$ that corresponds to a nearest neighbor distance of 8.52 A^o between two adsorbates), and one adsorbate per four unit cell for the (6,6) armchair SWNT (*i.e.* $c_s \sim 4c$ that corresponds to a nearest neighbor distance of 9.86 A^o between two adsorbates). In order to deduce the changes in the electronic structure of the bare tubes induced by the adsorbates, we first present in Fig. 4.5 the electronic structure and total density of states (TDOS) of the bare (8,0)

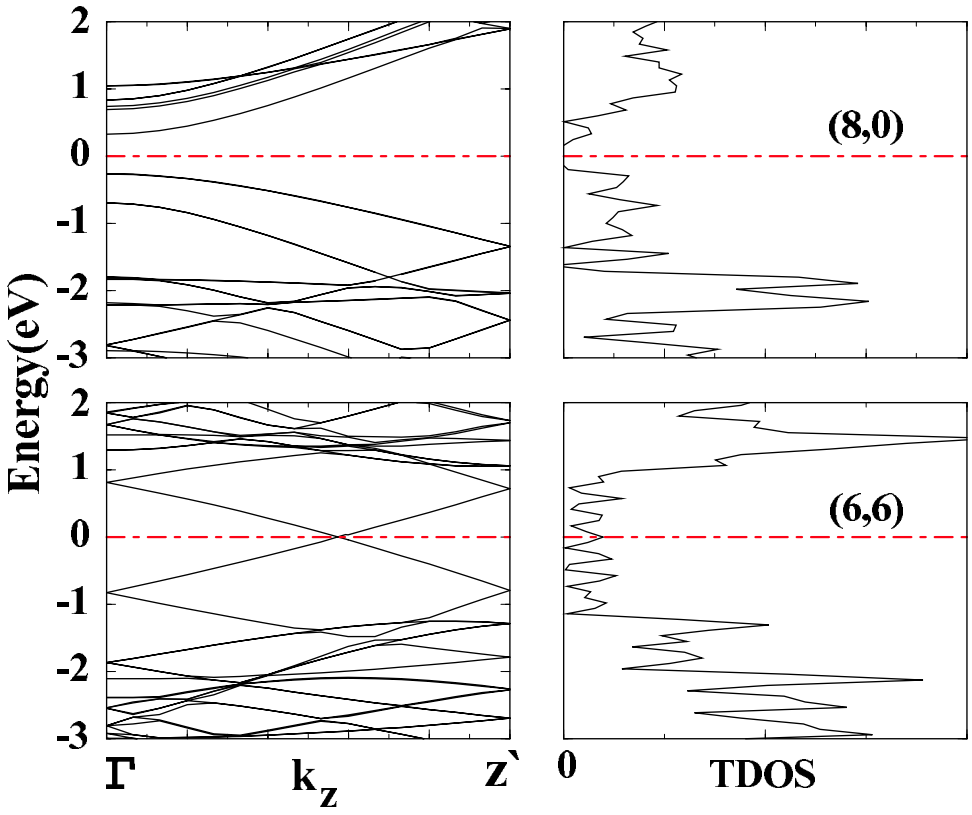

Figure 4.5: Energy band structures and total density of states (TDOS) of bare tubes with fully relaxed atomic structure. (a) Electronic structure of the semiconducting (8,0) zigzag SWNT calculated for the double primitive unit cells consisting of 64 C atoms. (b) same for the metallic (6,6) armchair SWNT calculated for the quadruple primitive unit cells including 96 C atoms. Zero of energy is set at the Fermi level E_F.

and bare (6,6) SWNTs calculated for double and quadruple primitive unit cells, respectively. Note that upon enlarging the unit cells for twice and four times the corresponding Brillouin zone is reduced by 1/2 and 1/4, respectively. Accordingly, the energy bands are zone-folded. We see that the direct band gap of the (8,0) zigzag SWNT occurs at the center of the Brillouin zone, but the (6,6) armchair tube is a metal with bands crossing at E_F.

4.5.1 Semiconducting (8,0) SWNT

The localized states are relevant for the doping of a semiconducting SWNT. Depending on their position relative to the band edges they are specified as donor states (if they are close to the edge of the conduction band E_C) or as acceptor states (if they can occur close to the edge of the valence band, E_V). The latter case is also known as hole doping. Whether the associated localized state is a donor or acceptor state can be inferred from the energy position of the band in the gap. We first consider Na, Al, C, and Si, which are adsorbed individually on the (8,0) SWNT with a repeat period of $2c$, and give rise to spin-paired, non-magnetic ground state. In Fig. 4.6 we present the calculated band structures and LDOS at the adatoms.

Calculated band structure of SWNT with Na adsorbed at the H-site forming a regular chain with a lattice parameter (or interatomic distance) $a = c_s \sim 2c$ yields a half-filled band. This band is normally the first empty conduction band of the tube. Since the $4s$-valence electron of Na has low ionization energy, it is donated to the SWNT to occupy the empty conduction band. As a result, this empty band which is gradually populated and also modified upon the adsorption of Na, hence the SWNT becomes metallized. Similarly, calculated band structure of SWNT with Al adsorbed at the H-site forming a regular chain structure gives rise to a half-filled band derived from the empty conduction band of SWNT. Therefore, the localized state due to an adsorbed individual Al atom is a donor state.

In the case of C, a small gap occurs between the bands derived from adsorbate states. The empty and filled bands just above and below E_F are derived from C adatom with significant contribution of SWNT. Si yields almost fully occupied band in the band gap, and almost empty band at the bottom of the conduction band. The dispersion of bands for Si adsorbed on the H-site displays differences from that of the C adatom adsorbed at the Z-site. However, overall behavior of state densities are similar.

In Fig. 4.7 the spin-polarized band structure and TDOS of adsorbed transition

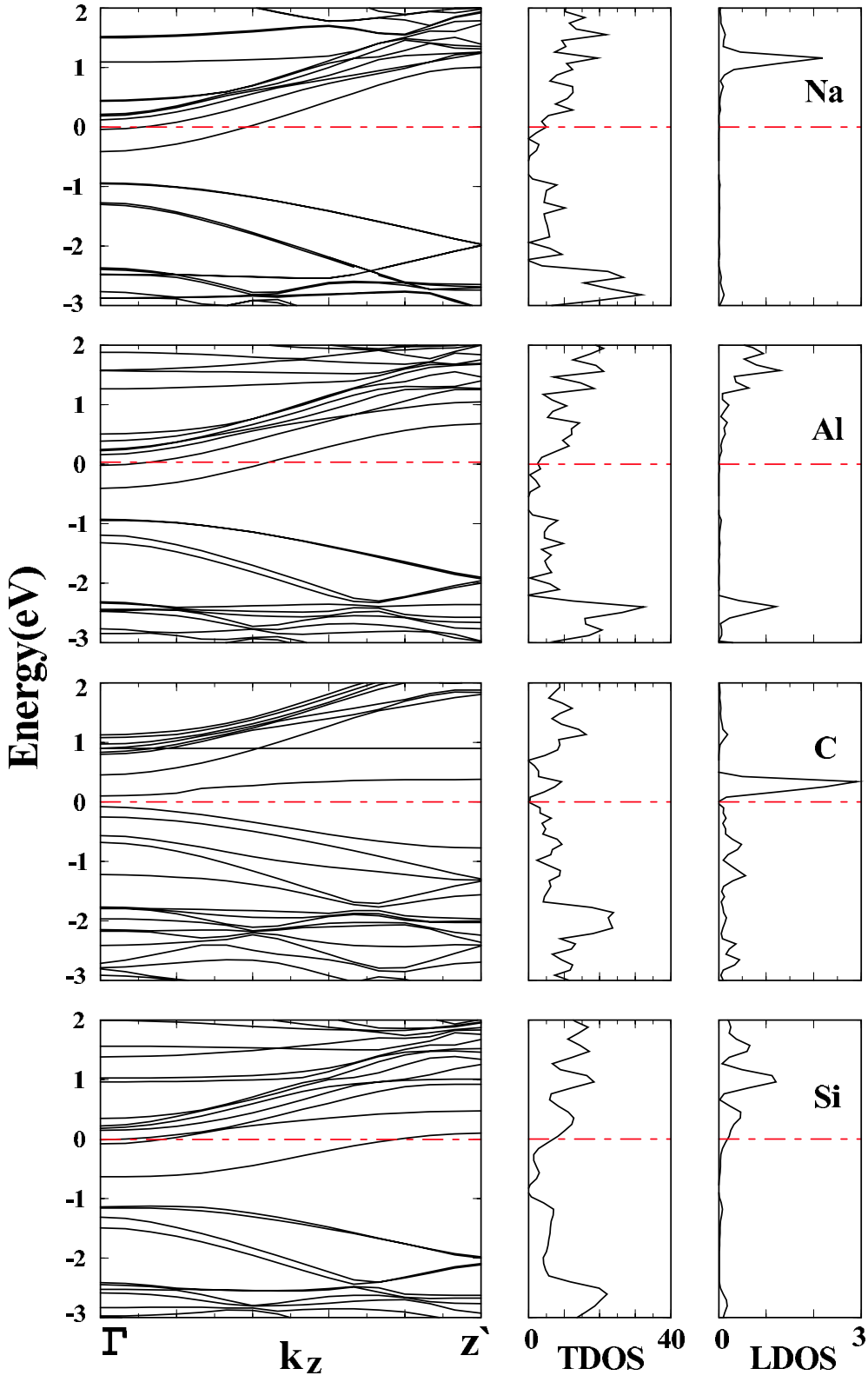

Figure 4.6: Energy band structures, TDOSs and LDOSs of single Na, Al, C, Si adsorbed on a zigzag (8,0) tube. LDOSs calculated at the adsorbate. Zero of energy is set at the Fermi level. Na, Al, and Si are adsorbed at the H-site; C is adsorbed at the Z-site.

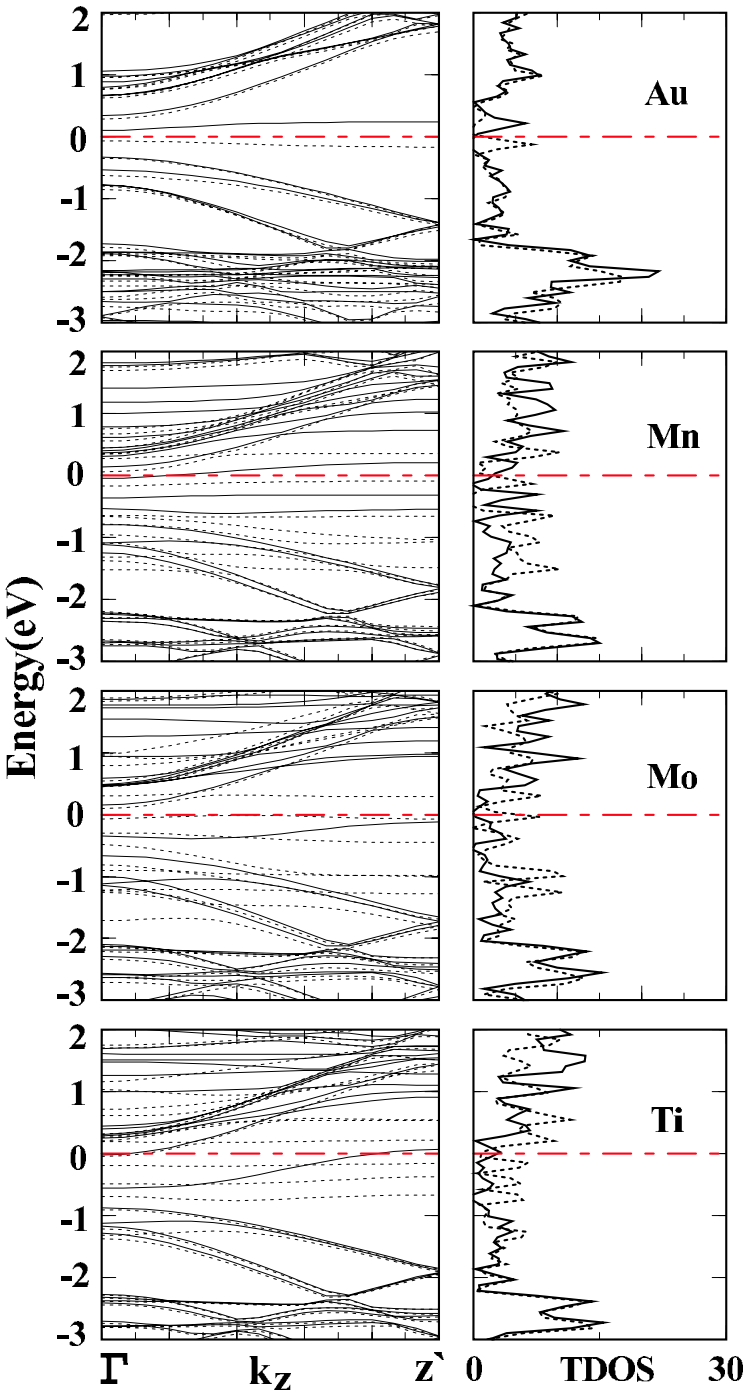

Figure 4.7: Energy band structures and total density of states (TDOS) of single Au, Mn, Mo, and Ti adsorbed on a zigzag (8,0) tube. Zero of energy is set at the Fermi level. Bands and state density of spin-up and spin-down states are shown by dotted and continuous lines, respectively. Mn, Mo, Ti are adsorbed at the H-site; and Au is adsorbed at the T-site.

metal atoms (*i.e.* Au, Mn, Mo, and Ti) display a different situation due to magnetic ground state. Au yield two bands in the band gap of bare SWNT; these are filled Au spin-up and empty spin-down bands. This is in compliance with the calculated magnetic moment of 1.02 μ_B per adsorbed Au atom. There is a small band gap of $\sim$0.2 eV between these Au bands. Comparing these bands with those of bare (8,0) SWNT in Fig. 4.5(a), we see that the adsorbtion of Au did not induce significant modification in the bands of (8,0), except the Au $6s(\uparrow)$ and Au $6s(\downarrow)$ bands in the gap, give rise to two sharp peaks below and above E_F, respectively in TDOS. That the contribution of SWNT states to these peaks is minute and the band gap between the conduction and valence bands of SWNT is practically unchanged confirms the weak interaction between Au and SWNT. Filled Au $5d(\uparrow)$ and $5d(\downarrow)$ bands occur in the valence band of SWNT 2 eV below E_F. Free Mn atom has normally $(3d^5)(4s^2)$ configuration and has magnetic moment of $5\mu_B$. The flat spin-up and spin-down bands of Mn occur in the band gap and near the edge of valence band. The band gap between the highest occupied spin-up and lowest empty spin-down band is very small (< 0.1 eV). The d-bands of adsorbed Mo occur in the band gap and near the top of the valence band of SWNT. The band gap between the highest occupied spin-up band and the lowest spin-down band is $\sim$0.2 eV. Thus, the highest occupied state due to Mo occurs near the edge of conduction band. The number of $4d(\uparrow)$ bands confirm that the net magnetic moment of Mo adsorbed SWNT is $4\mu_B$ per cell. Three bands formed from Ti $3d(\uparrow)$ are fully occupied and accommodate 3 electrons of adsorbed Ti atom. Other Ti $3d(\uparrow)$ bands occur above E_F, but they overlap with the conduction band of SWNT. The dispersive and almost fully occupied spin-down band is formed from the states of carbon and hence derived from the conduction band of the bare SWNT. The SWNT is metallized upon Ti adsorbtion, since this band cross the Fermi level and also overlap with the other conduction bands. This situation is in accordance with the Mulliken analysis, which predicts electrons are transferred from Ti to SWNT.

4.5.2 Metallic (6,6) SWNT

As far as the adsorption of foreign atoms are concerned, the main difference between the semiconducting (8,0) tube and metallic (6,6) tube have been the relatively lower binding energies calculated for the adsorption on the latter so far. This trend has been attributed to the curvature effect. In this section we explore whether the metallicity of the tube can influence the electronic structure in any essential manner. In Fig. 4.8 the energy band structures of Au, Mo and Ti adsorbed on the (6,6) tube are shown. In the case of Au the band structure of the bare (6,6)tube is not affected except that a small gap is opened between the π-valence and π^*-conduction band crossing at E_F. The gap-opening is the direct consequence of the symmetry as explained by Delenay et al.[71] In this gap, we see Au spin-up and Au spin-down bands, which give rise two peaks at both sides of E_F. Overall behavior of TDOS near E_F appears to be similar for the adsorption of Au on both (8,0) and (6,6) tube. We see, however, significant modifications in the band structure of bare (6,6) upon the adsorption of Mo and Ti. Although the overall behavior of state densities near E_F is similar for the adsorption of individual Mo and Ti on both (8,0) and (6,6) tube, very small band gap between spin-up and spin-down bands of Mo adsorbed in (8,0) tube disappears when it is adsorbed on the (6,6) tube.

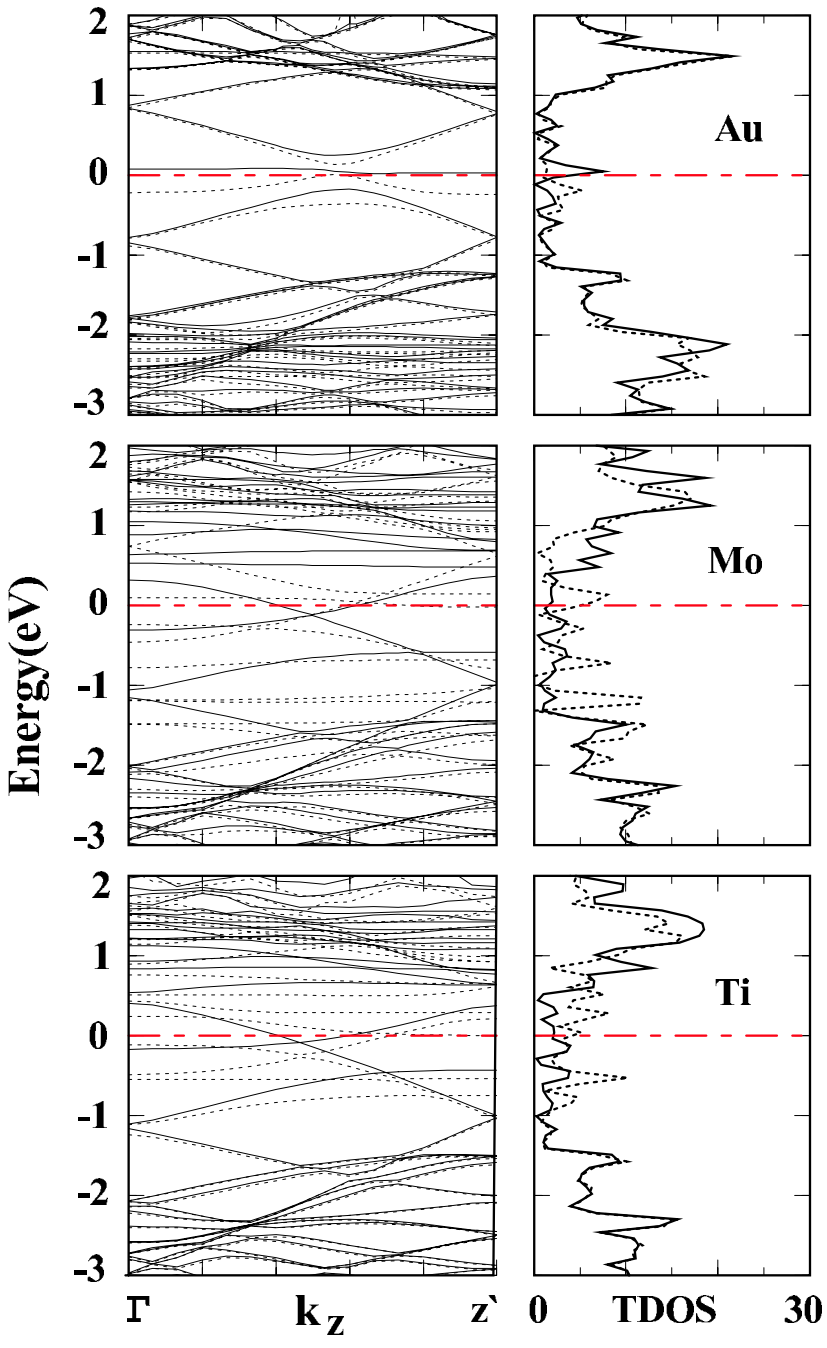

Figure 4.8: Energy band structures and total density of states (TDOS) of single Au, Mo, and Ti adsorbed on a armchair (6,6) tube. Zero of energy is set at the Fermi level. Bands and state density of spin-up states and spin-down states are shown by dotted and continuous lines, respectively. Mo, Ti are adsorbed at the H-site; Au is adsorbed at the T-site.

Chapter 5

Conclusions and Future Work

Our work, which is the most extensive ab-initio study on the functionalization of carbon nannotubes, reveals a number of interesting physical properties that can be generated by the adsorption of single atom on a SWNT. We believe that these findings are essential for a better understanding of adatom-SWNT interaction, coating and nanodevice design. Here we emphasize some of the important findings by way of conclusion:

1. Changes in the physical properties depend on the valency of the adsorbate.
2. Na having 3s-valence state with small ionization potential donates this valence electron to the empty conduction band of semiconducting SWNT. Therefore, adsorption of Na results in the metallization of the (8,0) tube.
3. Similar effects occur upon the adsorption of Al. The local density analysis shows that the band crossing the Fermi level (See Fig. 4.6) derives mainly from the (8,0) SWNT which was semiconductor before adsorbing Al atom.
4. However, adsorption of individual transition metal atoms gives rise to dramatically different results. Because of their occupied d-states, the transition metal adsorbed SWNT has a magnetic ground state. Also depending on the half-filled d-orbitals the binding energies show interesting behavior.

5. Mg ($4s^2$) and Zn ($3d^{10}4s^2$) which have closed shells give almost non-binding. This also confirms the relation between the half-filled orbitals and strength of binding.

6. In some of the cases (for example Au), adsorbed individual transition atom gives rise to a band gap between spin-up and spin-down bands within the supercell geometry. Ti , that leads to a metal, appears to be an exception. Another important property that is specific for Ti is its continuous coating of SWNT [16]. This should be related to both Ti-Ti and Ti-SWNT interaction. Whether the Ti covered SWNT leads to regular atomic structure, and the nanowire produced from Ti covered SWNT allows ballistic quantum transport are important issues requiring further investigations.

7. Good conductors which are widely used in micro-electronics such as Au, Ag and Cu have very weak binding. This suggests the possibility of replacing them with transition elements such as Ti, V, Ni and Co which have strong binding, in nano-electronic applications.

8. The adsorption of transition metal atoms on the (6,6) tube exhibits similar trends as the (8,0) tube, except that the binding energies in the former are consistently smaller. We attribute this behavior to the relatively smaller curvature of the (6,6) tube.

9. Si which is also a group IV element like C can be substituted into SWNT. The resulting structure is stable but energetically unfavorable and most probably it corresponds to a local minimum in Born-Oppenheimer surface.

10. Two SWNTs can be connected by C adatoms. The C atom between the tubes four directional bonds with bond length comparable to diamond crystal. The resulting geometry is stable and adding C atom metallizes whole system which was semiconducting before.

    As a final words, depending on our results we can predict that higher coverage and decoration of adsorbed foreign atoms can produce nanostructures (such as nanomagnets, nanometer size magnetic domains, 1D conductors and thin metallic connects, and electronic devices) which may find interesting technological application, such as spintronics and high density data

storage, and interconnects between devices. The d-orbitals of the transition metal atoms are responsible for relatively higher binding energies, which display an interesting variation with the number of filled d-states.

As a future work, we are planning to investigate the coverage of SWNTs by various transition metal atoms according to given pattern and investigate the magnetic interactions thereof.

Bibliography

[1] T. A. Edison, US Patent **470**, 925 (1892).

[2] T. Koyoma, Carbon **10**, 757 (1972).

[3] G. G. Tibbetts, Appl. Phyd. Lett. **42**, 666 (1983).

[4] H. W. Kroto, J. R. Heath, S. C. O'Brien, R. F. Curl, and R. E. Smalley, Nature (London) **318**, 162 (1985).

[5] M. S. Dresselhaus, Dod Workshop in Washington, DC (December 1990).

[6] S. Iijima, Nature (London) **354**, 56 (1991); S. Iijima, T. Ichihashi, and Y Ando, *ibid* **356**, 776 (1992).

[7] M. S. Dresselhaus, G. Dresselhaus, and P. C. Eklund, *Science of Fullerenes and Carbon Nanotubes* (Academic Press, San Diego, 1966).

[8] R. Saito, G. Dresselhaus and M. S. Dresselhaus, *Physical Properties of Carbon Nanotubes*; Imperial College Press, London (1998).

[9] J. W. G. Wilder, L. C. Venema, A. G. Rinzler, R. E. Smalley and C. Dekker, Nature **391**, 59 (1998).

[10] L. Chico, V. H. Crespi, L. X. Benedict, S. G. Louie, and M. L. Cohen, Phys. Rev. Lett. **76**, 971 (1996)

[11] M.F.Yu *et al.*, Science, **287**, 637 (1998).

[12] J.P. Salvetat *et al.*, Appl. Phys. A **69**, 255 (1999).

[13] E. Durgun, S. Dag, V.M.K. Bagci, O. Gülseren, T. Yildirim, S. Ciraci, Phys. Rev. B **67**, R201401 (2003).

[14] E. Durgun, S. Dag, O. Gülseren and S. Ciraci, submitted to J. of Phys. Chem. B.

[15] S. Dag, O. Gülseren, T. Yildirim, and S. Ciraci, Phys. Rev. B **67**, 165424 (2003)

[16] S.Dag, E. Durgun and S. Ciraci, Phys Rev. B (Rapid Communication), accepted for publication.

[17] H. Dai, J. H. Hafner, A. G. Rinzler, D. T. Colbert, and R. E. Smalley, Nature **384**, 147 (1996).

[18] S. B. Aranson *et al.*, Appl. Phys. Lett. **75**, 2842 (1999).

[19] S.J. Tans, A.R.M. Verscheuren and C. Dekker, Nature (London), **393**, 49 (1998); A. Bachtold, P. Hadley, T. Nakanishi, and C. Dekker, Science **294**, 1317 (2001).

[20] S. Heinze, J. Tersoff, R. Martel, V. Derycke, J. Appenzeller, and Ph. Avouris, Phys. Rev. Lett. **89**, 106801 (2002).

[21] M. Bockrath, D. H. Cobden, P. McEuen, N. G. Chopra, A. Zettl, A. Thess, and R. E. Smalley, Science 275, 1922 (1997).

[22] S. J. Tans, M. H. Devoret, H. Dai, A. Thess, R. E. Smalley, L. J. Geerligs, and C. Dekker, Nature (London) 386, 474 (1997)

[23] R.E Pierls, Ann. Phys. 4, 121 (1930)

[24] T. W. Ebbesen, H. J. Lezec, H. Hiura, J. W. Bennett, H. F. Ghaemi, and T. Thio *et al.*, Nature **382**, 54 (1996).

[25] C. Zhou, J. Kong, and H. Dai, Phys. Rev. Lett. **84**, 5604 (2000).

[26] Y. Zhang and H. Dai, Appl. Phys. Lett. **77**, 3015 (2000); Y. Zhang, N.W. Franklin, R.J. Chen, and H. Dai, Chem. Phys. Lett. **331**, 35 (2000).

[27] N. Hamada, S. Sawada and A. Oshiyama, Phys. Rev. Lett. **68**, 1579 (1992).

[28] A. Thess *et al.*, Science **273**, 483 (1996)

[29] C. Journet, W. K. Maser, P. Bernier, A. Loiseau, M. L. Chapelle, S. Lefrant, P. Deniard, R. Lee, and J. E. Fischer, Nature (London) **388**, 756 (1997)

[30] S. Seraphin, D. Zhou, J. Jiao, J. C. Withers, and R. Lofty, Carbon **31**, 685 (1993)

[31] J. A. Floro, S. M. Rossnagel, and R. S. Robinson, J. Vac. Sci. Technol. **A1**, 1398 (1983).

[32] M. Born and J. R. Oppenheimer, Ann. der Phys. **84**, 457 (1927).

[33] A. Messiah, *Quantum Mechanics* (Amsterdam, North-Holland, 1961).

[34] D. R. Hartree, Proc. Cambridge. Philos. Soc. **24**, 89 (1928).

[35] V. Fock, Z. Phys. **61**, 126 (1930).

[36] J. C. Slater, Phys. Rev. **35**, 210 (1930).

[37] L. H. Thomas, Proc. Cambridge. Philos. Soc. **23**, 542 (1927).

[38] E. Fermi, Z. Phys. **48**, 73 (1928).

[39] P. Hohenberg and W. Kohn, Phys. Rev. **136**, B864 (1964)

[40] W. Kohn and L. J. Sham, Phys. Rev. **140**, A1133 (1965).

[41] R. O. Jones and O. Gunnarson, Rev. Mod. Phys. **61**, 689 (1989)

[42] J. P. Perdew and Y. Wang, Phys. Rev. B, **45**, 13244 (1991).

[43] C. Kittel *Introduction to Solid State Physics* (Wiley and Sons, New York, 1996).

[44] H.J. Monkhorst and J.D. Pack, Phys. Rev. B**13**, 5188, (1976).

[45] N. Agräait, J.G. Rodrigo, and S. Vieira, Phys. Rev. B**47**, 12345 (1993).

[46] H. Ohnishi, Y. Kondo, and K. Takayanagi, Nature (London) **395**, 783 (1998).

[47] A.I. Yanson, G.R. Bollinger, H.E. Brom, N. Agräit, and J. M. Ruitenbeek, Nature (London) **395**, 783 (1998).

[48] S. Ciraci and E. Tekman, Phys. Rev B**40**, R11969 (1989);E. Tekman, S. Ciraci, Phys. Rev B**43**, 7145 (1991).

[49] S. Ciraci, A. Buldum and I.P. Batra, J. Phys.: Condens. Matter **13**, R537 (2001).

[50] A. Buldum, S. Ciraci, C.Y. Fong, J. Phys.: Condens. Matter **12**, 3349 (2000); A. Buldum, D.M. Leitner, and S. Ciraci, Europhys. Lett. **47**, 208 (1999).

[51] A. Ozpineci and S. Ciraci, Phys. Rev. B**63**, 125415 (2001).

[52] O. Gülseren, F. Ercolesi and E. Tosatti, Phys. Rev. Lett. **80** 3775 (1998); E. Tosatti and S. Prestipino, Science **289**, 561 (2000).

[53] H. Dai, E.W. Wong, Y.Z. Lu, S. Fan, C.M. Lieber, Nature(London) **375**, 769 (1995); W.Q. Han, S.S. Fan, Q.Q. Li, Y.D. Hu, Science **277**, 1287 (1997).

[54] H.T. Soh, C. Quate, A.F. Morpurgo, C.M. Marcus, J. Kong and H. Dai, Appl. Phys. Lett. **75**, 627 (1999); C. Zhou, J. Kong, and H. Dai, Appl. Phys. Lett. **76**, 1597 (2000).

[55] R. Martel, V. Derycke, C. Lavoie, J. Appenzeller, K.K. Chan, J. Tersoff, and Ph. Avouris, Phys. Rev. Lett. **87** 256805 (2001).

[56] V.M.K. Bagci, O. Gülseren, T. Yildirim, Z. Gedik, and S. Ciraci, Phys. Rev. B**66**, 045409 (2002).

[57] I.O. Kulik, T. Hakioglu, and A. Barone, Europ. Phys. Journal, B**30**, 219 (2002).

[58] X.X. Zhang, G.H. Wen, S. Huang, L. Dai, R. Gao, and Z.L. Wang, Journal of Magnetism and Magnetic Materials, **231**, L9 (2001); B.C. Satishkumar, A. Govindaraj, P.V. Vanitha, A.K. Raychaudhuri, and C.N.R. Rao, Chem. Phys. Lett. **362**, 301 (2002).

[59] T. Yildirim, O. Gülseren, and S. Ciraci, Phys. Rev. B**64**, 075404 (2001); O. Gülseren, T. Yildirim, and S. Ciraci, Phys. Rev. B**66**, 121401 (2002).

[60] J.P. Perdew, J.A. Chevary, S.H. Vosko, K.A. Jackson, M.R. Pederson, D.J. Singh and C. Fiolhois, Phys. Rev. B**46**, 6671 (1992).

[61] O. Gülseren, T. Yildirim and S.Ciraci, Phys. Rev. Lett **87**, 116802, (2001).

[62] O. Gülseren, T. Yildirim, and S. Ciraci, Phys. Rev. B**65**, 155410 (2002); O. Gülseren, T. Yildirim, S. Ciraci and C. Kilic, Phys. Rev. B**65**, 153405 (2002).

[63] D. Vanderbilt, Phys. Rev. B **41**, 7892 (1990).

[64] E.M. Lifshitz, Zh. Eksp. Teor. Fiz. **29**. 94 (1956) [Sov. Phys. JETP **2**. 73 (1956)].

[65] T. A. Halgren, J. Am. Chem. Soc. **114**. 7827 (1992).

[66] C. E. Moore, *Atomic Energy Levels* U.S. National Bureau of Standards, Washington D.C. 1971.

[67] P. Soderlind, O. Eriksson, J.M. Wills, and A.M. Boring, Phys. Rev. B **48**, 5844 (1993).

[68] J. Friedel, The Physics of Metals, edited by J. M. Ziman (Cambridge University Press, New York, 1969); D.G. Pettifor, in Solid State Physics, edited by H. Ehrenreich and D. Turnbull (Academic, New York, 1987). Vol. **40**, p43.

[69] X. Blase, L.X. Benedict, E.L. Shirley and S.G. Louie, Phys. Rev. Lett. **72**, 1878 (1994)

[70] R. J. Baierle, S. B. Fagan, R. Mota, A.J.R. Silva, and A. Fazzio, Phys. Rev. B **64**, 085413 (2001).

[71] P. Delaney, H.J. Choi, J. Ihm, S.G. Louie, M.L. Cohen, Nature(London) **391**, 466 (1998).

Publications coauthored by Engin Durgun

1. **"Systematic study of adsorption of single atoms on a carbon nanotube"**, *E.Durgun*, S. Dag, V. M. K. Bagci, O. Gülseren, T. Yildirim, and S. Ciraci, Physical Review B (Rapid Communication) **67**, 201401 (2003).

2. **"High conducting, crystalline nanowires obtained from titanium covered carbon nanotubes"**, S. Dag, *E.Durgun* and S. Ciraci, Physical Review B (Rapid Communication), accepted for publication.

3. **"Energetics and electronic structure of individual atoms adsorbed on carbon nanotubes"**, *E.Durgun*, S. Dag, S. Ciraci and O. Gülseren, submitted to Journal of Physical Chemistry B.

4. **"Theoretical Models for Nanodevices and Nanomagnets Based on Single-Wall Carbon Nanotubes"**, S. Ciraci, O. Gülseren, T. Yildirim, S. Dag, *E.Durgun*, Proceedings of NATO-ASI (Nanoengineered Nanofibrous Materials) Kluwer (2003).

5. **"Functionalization of Carbon Nanotubes: Deformation, Coating, Contacts and Device Applications"**, O. Gülseren, T. Yildirim, S. Dag, *E.Durgun*, S. Ciraci Proceedings of NATO-ASI (Nanoengineered Nanofibrous Materials) Kluwer (2003).